

**MAGNETIC COUPLING BETWEEN DC TACHOMETER AND MOTOR  
AND ITS EFFECT ON MOTION CONTROL IN THE PRESENCE OF  
SHAFT COMPLIANCE**

by

Shorya Awtar

A Thesis Submitted to the Graduate  
Faculty of Rensselaer Polytechnic Institute  
In Partial Fulfillment of the  
Requirements for the Degree of  
MASTER OF SCIENCE

Approved:

---

Professor Kevin C. Craig  
Thesis Advisor

Rensselaer Polytechnic Institute  
Troy, New York

August 2000

## TABLE OF CONTENTS

<b>LIST OF FIGURES</b> .....	iv
<b>LIST OF TABLES</b> .....	viii
<b>ACKNOWLEDGEMENTS</b> .....	ix
<b>ABSTRACT</b> .....	x
<b>1. INTRODUCTION</b> .....	1
<b>2. EXPERIMENTAL SET-UP</b> .....	3
2.1 System Description.....	3
2.2 Component Specification.....	4
<b>3. CONVENTIONAL TACHOMETER MODEL AND ITS DEFICIENCY</b> .....	7
<b>4. MODELING OF D.C. MACHINES</b> .....	12
4.1 D.C. Motor.....	13
4.2 D.C. Tachometer.....	17
4.3 Coupled D.C. Motor-Tachometer System.....	20
<b>5. EXPERIMENTAL VERIFICATION OF THE PROPOSED MODEL</b> .....	30
5.1 Discussions on the proposed Tachometer model.....	33
<b>6. TYPICAL APPLICATION: MOTION CONTROL IN PRESENCE OF SHAFT COMPLIANCE</b> .....	35
<b>7. CONTROL SYSTEM DESIGN</b> .....	42
7.1 Introduction.....	42
7.2 Colocated and Noncolocated Control.....	44
7.2.1 Two-mass single-spring system.....	44
7.2.2 Open-loop characteristics: Physical Significance of poles and zeros.....	47

7.2.3	Close-loop characteristics: Stability Analysis.....	51
7.2.4	Multiple mass systems.....	66
7.3	Tachometer-Motor-Load System.....	70
<b>8.</b>	<b>CONCLUDING REMARKS AND FUTURE WORK.....</b>	<b>83</b>
	<b>REFERENCES.....</b>	<b>85</b>

## LIST OF FIGURES

Fig. 2.1	Schematic of Experimental Set-up.....	3
Fig. 3.1	Physical model of the motor-tachometer system.....	7
Fig. 3.2	Effect of damping on the zeros and poles of a system.....	8
Fig. 3.3	Comparison of the analytically-predicted and experimentally-obtained frequency response plots for the motor-tachometer system.....	10
Fig. 4.1	Electrical circuit diagram for a D.C. Motor.....	14
Fig. 4.2	Physical model for a D.C. motor.....	14
Fig. 4.3	Interaction between two magnetic fields.....	15
Fig. 4.4	Physical model for a D.C. tachometer.....	18
Fig. 4.5(a)	Angular orientations of the motor and tachometer permanent magnets.....	21
Fig. 4.5(b)	Motor and Tachometer fields.....	21
Fig. 4.6(a)	Magnetic Fields present in the Tachometer.....	22
Fig. 4.6(b)	Magnetic Fields present in the Motor.....	23
Fig. 4.7	Transformer effect between the motor armature coil and the tachometer armature coil.....	25
Fig. 5.1	Comparison of the analytically-predicted and experimentally-obtained frequency response plots for the motor-tachometer system.....	31
Fig. 6.1	Motor-tachometer-load system.....	36
Fig. 6.2	Physical Model of the motor-tachometer-load system.....	37
Fig. 6.3	$V_{tach}/V_{in}$ : Comparison of experimental frequency response and predicted frequency response using conventional model.....	39
Fig. 6.3	$V_{tach}/V_{in}$ : Comparison of experimental frequency response and predicted frequency response using proposed model.....	39
Fig. 7.1	Two-mass single-spring system.....	44

Fig. 7.2	Bode plot for $x_1 / F_{in}$ transfer function.....	45
Fig. 7.3	Bode plot for $x_2 / F_{in}$ transfer function.....	46
Fig. 7.4	System frequency response when excitation force is applied on mass-1.....	49
Fig. 7.5	Bode plot for $x_2 / x_1$ transfer function.....	50
Fig. 7.6(a)	Root-locus for the rigid body case ( $1/s^2$ ).....	52
Fig. 7.6(b)	Bode plots for the rigid body case ( $1/s^2$ ).....	52
Fig. 7.7(a)	Root-locus for the rigid body case with lead compensation ( $\frac{s+2}{s^2}$ ).....	53
Fig. 7.7(b)	Bode plot for the rigid body case with lead compensation ( $\frac{s+2}{s^2}$ ).....	54
Fig. 7.8(a)	Root-locus plot for the uncompensated collocated system ( $\frac{s^2+z_1^2}{s^2(s^2+p_1^2)}$ )....	55
Fig. 7.8(b)	Bode plots for the uncompensated collocated system ( $\frac{s^2+z_1^2}{s^2(s^2+p_1^2)}$ ).....	56
Fig. 7.9(a)	Root-locus plot for the compensated collocated system: $(s+2)\frac{s^2+z_1^2}{s^2(s^2+p_1^2)}$ .....	57
Fig. 7.9(b)	Root-locus plot for the compensated collocated system: $(s+2)\frac{s^2+z_1^2}{s^2(s^2+p_1^2)}$ .....	58
Fig. 7.10(a)	Root-locus for the uncompensated noncollocated system ( $\frac{1}{s^2(s^2+p_1^2)}$ )....	59
Fig. 7.10(b)	Bode plots for the uncompensated noncollocated system ( $\frac{1}{s^2(s^2+p_1^2)}$ )....	59
Fig. 7.11(a)	Root-locus plot for the lead compensated noncollocated system:	

$((s + 2) \frac{1}{s^2(s^2 + p_1^2)})$ .....	60
--	----

Fig. 7.11(b) Bode plots for the lead compensated noncolocated system:

$((s + 2) \frac{1}{s^2(s^2 + p_1^2)})$ .....	61
--	----

Fig. 7.12(a) Root-locus plot for the notch compensated noncolocated system.....62

Fig. 7.12(b) Bode plots for the notch compensated noncolocated system.....63

Fig. 7.13(a) Root-locus for the notch compensated noncolocated system in the presence of pole-zero flipping.....64

Fig. 7.13(b) Bode plots for the notch compensated noncolocated system in the presence of pole-zero flipping.....65

Fig. 7.14 Multiple-mass multiple-spring system.....66

Fig. 7.15 Four-mass three-spring system.....67

Fig. 7.16(a) Pole-zero flipping in a noncolocated system.....68

Fig. 7.16(b) Pole-zero flipping in a noncolocated system.....69

Fig. 7.17 Physical System and Physical Model.....70

Fig. 7.17(a)  $\frac{q_t}{T_m}$  : Root-locus for the tachometer-motor-load mechanical system.....72

Fig. 7.18 Root locus for (a) Uncompensated system (b) Lead compensated system.....73

Fig 7.19 Bode Plots for the system with lead compensation.....74

Fig 7.20 Block-diagram based representation of the open-loop tachometer-motor-load mechanical and electrical system.....76

Fig. 7.21 The tachometer-motor-load electromechanical system.....76

Fig. 7.22 Close-loop block diagram of the tachometer-motor-load electromechanical system...77

Fig. 7.23(a)	Root-locus plot (b) Bode plots for the uncompensated system.....	79
Fig. 7.24(a)	Root-locus plot for the lead compensated tachometer-motor-load electromechanical system.....	80
Fig. 7.24(a)	Root-locus plot for the lead compensated tachometer-motor-load electromechanical system.....	81

## LIST OF TABLES

Table 2.1	Specifications of the Electro-craft DC Motor Tachometer assembly.....	4
Table 2.2	Specifications of the Advanced Motion Controls PWM amplifier.....	5
Table 2.3	Specifications of the Power Supply.....	5
Table 3.1	List of symbols used in Section 3 .....	7
Table 4.1	List of symbols used in Section 4.1.....	13
Table 4.2	List of symbols used in Section 4.2.....	17
Table 4.3	List of symbols used in Section 4.3.....	20
Table 5.1	List of symbols used in Section 5.....	30
Table 6.1	List of symbols used in Section 6.....	35
Table 6.2	Comparison of experimentally observed and theoretically predicted (using the proposed model) zero and pole frequencies.....	40

## **ACKNOWLEDGEMENTS**

I am thankful to my thesis advisor Professor Kevin C. Craig for his guidance and support. I also wish to express my thanks to my colleagues, Celal Tufekci and Jeongmin Lee for their help during the course of this research.

## ABSTRACT

This thesis presents an accurate tachometer model that takes into account the effect of magnetic coupling in a DC motor-tachometer assembly. Magnetic coupling arises due to the presence of mutual inductance between the tachometer winding and the motor winding (a weak transformer effect). This effect is modeled and experimentally verified. Tachometer feedback is widely used for servo-control of DC motors. The presence of compliant components in the drive system, e.g., shafts, belts, couplings etc. may lead to close-loop instability which manifests itself in the form of high frequency ringing. To be able to predict and eliminate these resonance related problems, it is essential to have an accurate tachometer model. This thesis points out the inadequacies of the conventional tachometer model, which treats the DC tachometer as a ‘gain’ completely neglecting any associated dynamics. It is shown that conventional models fail to predict the experimental system dynamics response for high frequencies. The exact tachometer model identified in this research is incorporated in the modeling of a system that has multiple flexible elements, and is used for parameter identification and feedback motion control. Predictions using this new model are found to be in excellent agreement with experimental results. The effect of the tachometer dynamics on controller design is discussed in the context of system poles and zeros.

*Key words:* DC Tachometer model, DC motor motion control, shaft flexibility, sensor dynamics, system poles and zeros, shaft ringing.

## 1. INTRODUCTION

Closed-loop servo control of a DC motor-load system is a very common industrial and research application. Very often DC tachometers are used to provide velocity feedback for motion control [3, 4, 5]. In the presence of flexibility in the system, e.g., a compliant motor-load shaft or a flexible coupling, this exercise in servo control becomes quite involved since finite shaft stiffness introduces resonance and shaft ringing. These are highly undesirable effects that can be eliminated by means of appropriate controller design. To be able to model, predict, and eliminate these high-frequency resonance problems, it is essential to have an accurate model for the entire system including the sensor.

There are papers in the literature that discuss the control system design for systems with mechanical flexibilities [4, 6, 8, 10]. There are also extensive discussions on colocated and non-colocated control in the literature. The problem is explained in terms of poles and zeros of the system [6, 7, 8, 9, 10]. All these discussions assume that a ‘perfect’ position or velocity signal is available for feedback and that sensor dynamics is negligible. Such an assumption might be acceptable for routine applications, but is not useful for high-performance applications. It is emphasized in this thesis that an accurate model for the sensor dynamics is necessary and should be incorporated in the control system design.

In the case of DC motor position and/or velocity control using tachometer feedback, the conventional tachometer model [1, 2, 3] is adequate for less demanding motion control exercises, but is ineffective for rendering high-speed and high-precision motion control. In fact, when this model was used to predict the frequency response of a system with multiple shaft flexibilities, it yielded erroneous results that did not agree with the experimental measurements. This led to an investigation leading to a more exact and accurate model for the DC tachometer. A thorough modeling analysis was carried out and it was found that the mutual inductance between the tachometer and motor windings, however weak, results in a magnetic coupling term in the expression for the voltage output of the tachometer. This effect is quantitatively studied and derived in this thesis,

and an enhanced tachometer model is obtained using the basic principles of electromagnetism. This model is then used to analyze a DC tachometer-motor-load system with multiple flexible elements. It is found that the new analytical predictions are in excellent agreement with the experimental measurements.

The consequence of this tachometer dynamics on the over-all system response is explained. It is seen that the tachometer dynamics influences the system transfer function in a way that is system dependent. This shall become clear in the following sections. We find that the tachometer dynamics contributes some additional zeros to the overall system transfer function. The number of these additional zeros depends on the system itself. The location of these zeros in the  $s$ -plane is determined by the relative orientation of the tachometer stator field with respect to the motor stator field. Having experimentally confirmed the model, we subsequently incorporate it in the feedback control design for DC motor motion control, which is the final objective of this entire exercise. The significance and implication of these additional zeros in terms of controller design is discussed in detail.

This thesis is organized in the following manner. Section 2 describes the experimental setup used for this research. Section 3 investigates the inconsistency presented by convention DC tachometer model. It is explained why the conventional model is inadequate for high performance servo-control design. A detailed description of Permanent Magnet DC machines is presented in Section 4. This covers the existing model and the derivation of a more accurate model. The experimental validation of the new model obtained in Section 4 is presented in Section 5. Section 6 describes the application of this model to an actual system with multiple flexible elements. Section 7 introduces the control design problems and issues related to it. A detailed discussion on colocated and noncolocated system is presented. These concepts are then extended to the tachometer-motor-load system, and the influence of tachometer dynamics on the control system design is explained. Finally, compensator designs for eliminating close-loop instability problems in the tachometer-motor-load system are discussed. Section 8 summarizes this research and lists the conclusions from this work.

## 2. EXPERIMENTAL SET-UP

### 2.1 System Description

To study and analyze the close-loop instability problems like shaft ringing in servo-systems, we used a Pitney-Bowes experimental test set-up. It consists of an integrated Permanent Magnet DC motor-tachometer assembly which drives a load inertia. A voltage-to-current PWM amplifier is employed to operate the motor in current mode. The system input is in the form of motor current. The system output, which is the tachometer voltage signal, may be used for system identification or for feedback motion control.

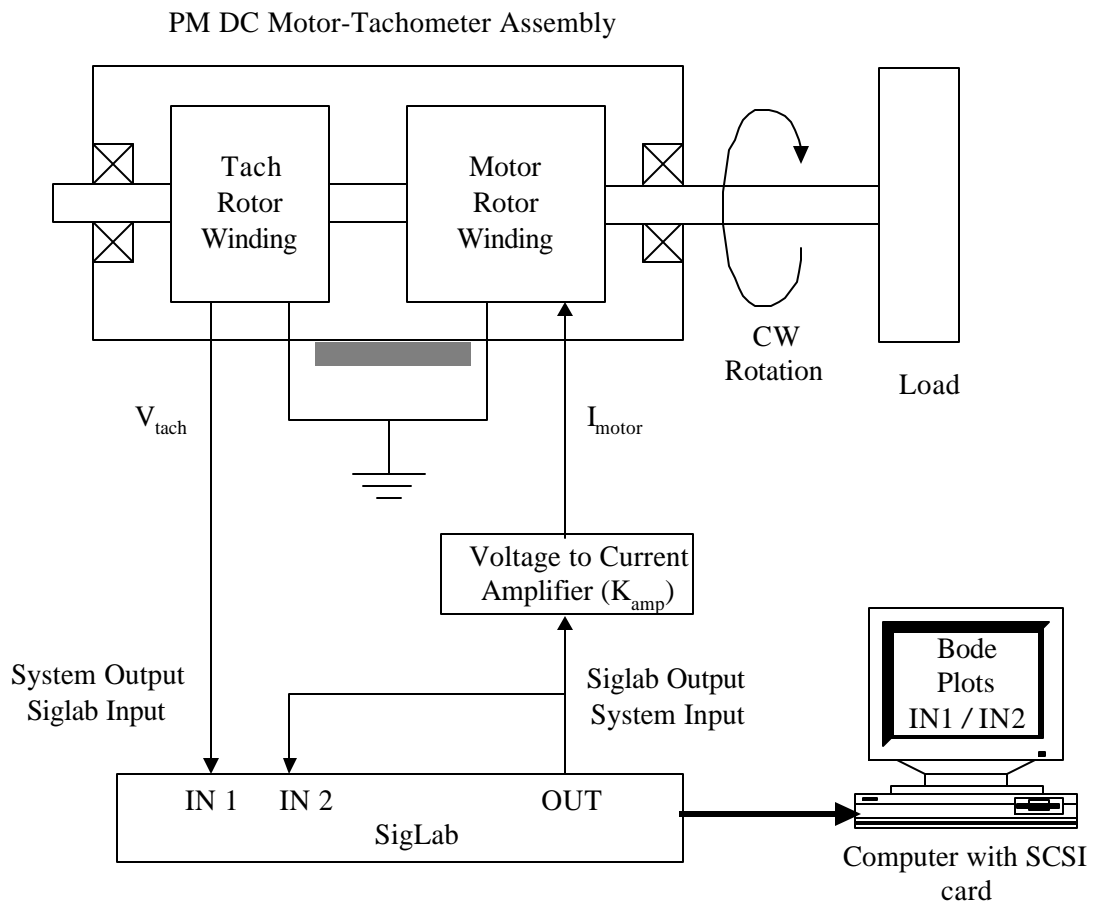


Figure 2.1 Schematic of the Experimental Set-up

The first phase of experimentation is performed to obtain frequency response plots for the above-described system, which is an exercise in system identification. For this purpose, we use a DSP tool, SigLab. SigLab sends a sine sweep over a user-specified frequency range as the system input in the form of a voltage signal to the current amplifier. At the same time it also collects the system output, which is the tachometer voltage in this case. Based on this input-output data, SigLab constructs the frequency response plots for the system. A schematic of this set-up is shown in Figure 2.1.

Motor polarity is chosen such that a positive motor current ( $I_m$ ) leads to a CW rotation of the rotor. Tachometer polarity is chosen such that a CW rotation of the rotor produces a positive tachometer voltage ( $V_{tach}$ ).

## 2.2 Component Specifications

### 1) DC Motor-Tachometer Assembly.

The motor and tachometer used for this set-up is a Permanent Magnet Brushed DC Motor-Tach assembly, Model No. 0288-32-003 from Electro-Craft Servo Products.

**Table 2.1 Specifications of the Electro-Craft 0288-32-003 DC Motor with Tachometer**

<b>Motor Characteristics</b>	<b>Units</b>	<b>Values</b>
Rated Voltage (DC)	volts	60
Rated Current (RMS)	amps	4
Pulsed Current	amps	29
Continuous Stall Torque	oz-in	50
Maximum Rated Speed	RPM	6000
Back EMF Constant	volts-/krpm	8.7
Torque Constant	oz-in/amp	11.8
Terminal Resistance	ohms	1.0
Rotor Inductance	mH	3.3

Viscous Damping Coefficient	oz-in/krpm	11.3
Rotor Inertia (including Tach)	oz-in-sec <sup>2</sup>	0.0078
Static Friction Torque	lb-in	0.19
Tachometer Voltage Constant	volts/krpm	14

## 2) Power Amplifier

The power amplifier used in this system is the Advanced Motion Controls PWM servo-amplifier, Model 25A8.

**Table 2.2 Specifications of the Advanced Motion Controls Model 25A8 PWM Amplifier**

<b>Power Amplifier Characteristics</b>	<b>Values</b>
DC Supply Voltage	20-80 V
Maximum Continuous Current	± 12.5 A
Minimum Load Inductance	200 μH
Switching Frequency	22 KHz ± 15%
Bandwidth	2.5 KHz
Input Reference Signal	± 15 V maximum
Tachometer Signal	± 60 V maximum

## 3) Power Supply

A DC power supply is used to drive the system.

**Table 2.3 Specifications of CSI/SPECO Model PSR-4/24 Power Supply**

<b>Power Supply Characteristics</b>	<b>Values</b>
Supply voltage	+24 Volts
Maximum Continuous Current	4 amps
Maximum Peak Current	7 amps

#### 4) DSP Tool

The DSP used for this experiment is the **SigLab 20-42** hardware/software tool from DSP Technology Inc. This DSP tool has the following features:

- DC to 20 kHz frequency range
- Fully alias-protected two or four-channel data acquisition system in one small enclosure
- Expandable from two to sixteen channels
- Ready to use Windows-based measurement and analysis software, coded in MATLAB
- On board real time signal processing provides 90dB alias protection and frequency translation (zoom)
- Integrated multifunction signal generation

Further information is available on the company website: <http://www.dspt.com>

### 3. CONVENTIONAL D.C. TACHOMETER MODEL AND ITS DEFICIENCIES

**Table 3.1 List of symbols used in this section**

Variable/Parameter	Symbol	Value
Motor angular position	$\theta_m$	-
Tachometer angular position	$\theta_t$	-
Motor armature inertia	$J_m$	43.77e-6 kg-m <sup>2</sup>
Tachometer armature inertia	$J_t$	11.35e-6 kg-m <sup>2</sup>
Motor-Tach shaft stiffness	$K$	1763 N-m/rad
Motor current	$i_m$	-
Motor torque	$T_m$	-
Motor torque constant	$K_t$	8.33e-2 N.m/A
Tachometer voltage	$V_{tach}$	-
Tachometer constant	$K_{tach}$	0.137 V/(rad/s)

For simplicity, we consider a DC motor-tachometer assembly without any external load inertia. A shaft of finite stiffness connects the tachometer armature and the motor armature. A physical model of this assembly with lumped parameters is shown in Figure 3.1.

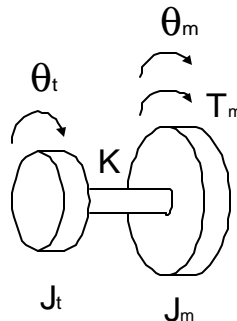


**Figure 3.1 Physical Model of Motor Tachometer assembly**

By drawing free-body diagrams for the two inertias  $J_t$  and  $J_m$ , and applying Newton's Second Law, we obtain the following transfer function:

$$\frac{q_t}{T_m} = \frac{K}{s^2 [J_t J_m s^2 + K (J_t + J_m)]} \quad (3.1)$$

It is worth-mentioning here that in the derivation of the above transfer function all frictional losses (Coulomb, viscous and structural) have been neglected. As shall become clear later in this thesis, the effect of damping terms is not important for the primary investigation that is being carried out. We are trying to identify the complex conjugate poles and zeros of the motor-tachometer system that arise due to the mechanical and electrical characteristics of the system. From a frequency response perspective, damping does not govern the existence of these poles and zeros. It only tends to reduce their intensity. This is illustrated in Figure 3.2.

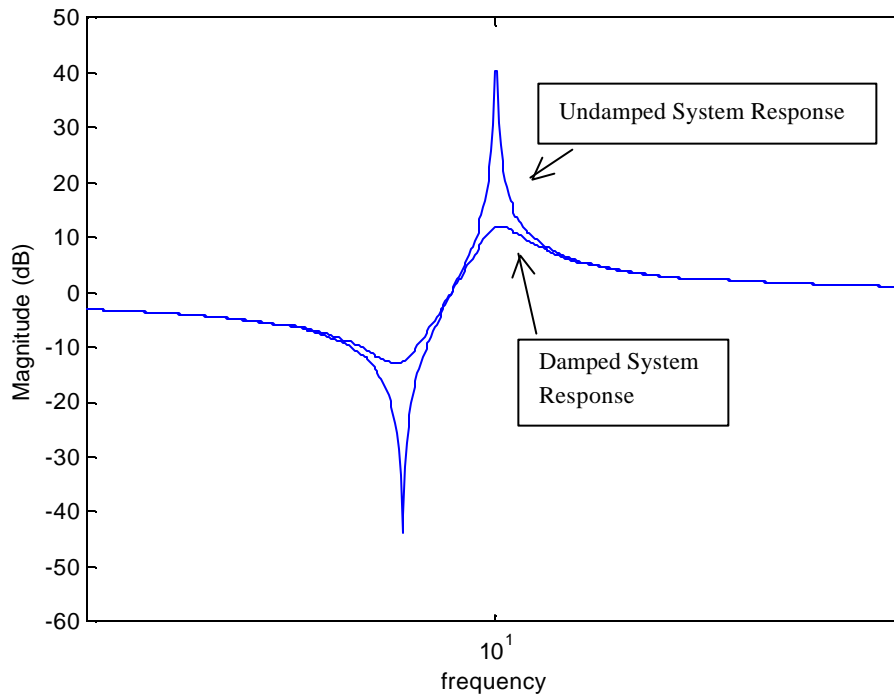


**Figure 3.2 Effect of damping on the zeros and poles of a system**

By presenting this argument, we justify the dropping out of damping terms in our model for the mechanical system at this stage. In the later part of this thesis though, when we talk about control system design, the signs of the damping terms become critical in terms of analyzing the close-loop system stability. At that stage, damping terms shall be introduced with due justification provided.

We now proceed with the pertinent analysis. Using the conventional DC motor and tachometer models, commonly found in text-books,

$$\begin{aligned} T_m &= K_t i_m \\ V_{tach} &= K_{tach} \dot{\theta}_t \end{aligned} \tag{3.2}$$

to model the motor-tachometer system described in Section 2, and the following overall system transfer function is obtained,

$$\frac{V_{tach}}{V_{in}} = \frac{K_{amp} K_{tach} K_t K}{s [ J_t J_m s^2 + K (J_t + K_m) ]} \tag{3.3}$$

This expression indicates the presence of one complex-conjugate pole pair. We get the frequency response plots for this transfer function using MATLAB. At the same time, we also obtain the experimental frequency response plots using SigLab as described in Section 2. The two sets of plots: analytical and experimental, are compared to check how well the theoretical transfer function predicts the actual system response (Figure 3.3).

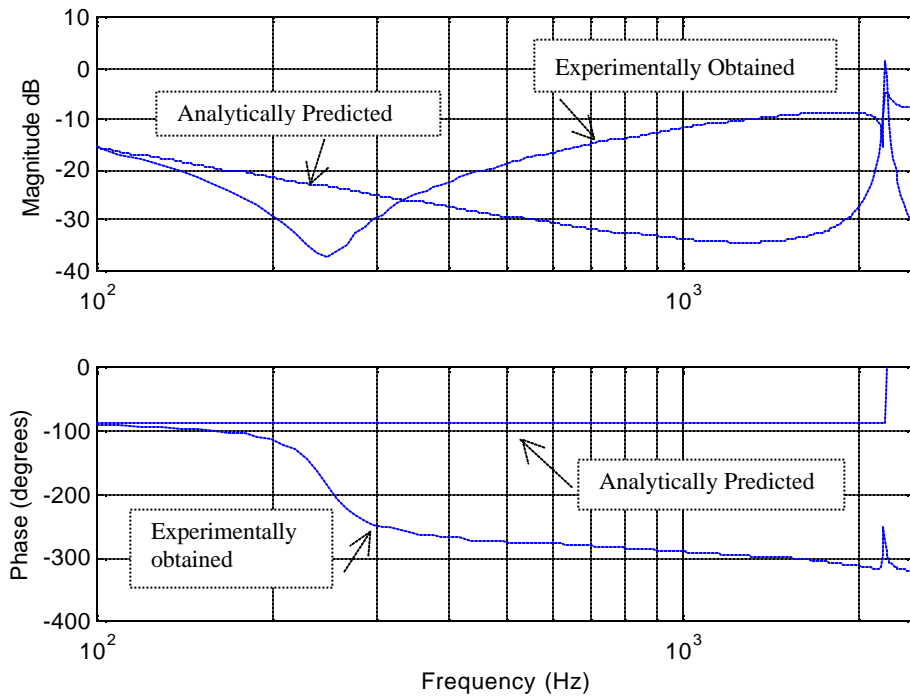


**Figure 3.3 Comparison of analytically-predicted and experimentally-obtained frequency response plots of the motor-tach system**

The following interesting observations are made from the above plots:

1. The analytically-predicted results match the experimental results in the low frequency range ( $< 100\text{Hz}$ ).
2. For higher frequencies the experimental results distinctly deviate from the predicted results and hence the model breaks down in the high frequency range.
3. The experimental results seem to indicate the presence of two pairs of complex-conjugate zeros in the system transfer function that are not predicted by the analysis.
4. The analysis does predict the system pole frequency quite accurately. The experimental results reveal one complex-conjugate pole pair and this is very close to the pole-pair predicted by the analysis.
5. In the experimental plot, we notice that the phase drops by  $180^\circ$  at the first zero frequency. This implies that the corresponding complex conjugate zero pair lies on

right side of the imaginary axis in the s-plane. This indicates the presence of negative damping term, which is unusual in a mechanical system.

Evidently, there are many discrepancies noticed in the above comparison that remain unexplained by the present analytical model for the system. This demands a closer inspection of the system modeling. Since expression (3.1) is derived by applying Newton's Second Law to a widely accepted physical model of a two-mass-one-spring system, its validity is almost certain. On the other hand, expressions (3.2) represent textbook models of idealized 'electromagnetically uncoupled' motor and tachometer respectively, which might be an over-simplification. Since their accuracy is questionable, we proceed to identify any electromagnetic phenomena that might give rise to some unidentified dynamics.

#### 4. MODELING OF D.C. MACHINES

We follow a thorough approach in deriving models for DC machines in order to make sure that we do not miss the influence of any weak, yet significant electromagnetic effect. We start from the fundamentals of electromagnetism to study the operation of DC machines. In the following analysis we have been particularly careful with the signs associated with various quantities, as any inconsistencies will lead to erroneous predictions.

In the following discussion, the fundamental laws of electromagnetism will be invoked frequently. These principles are listed here for the convenience of the reader:

1. Faraday's Law of Induction: The induced electro motive force, or emf, in a circuit is equal to the rate at which flux through the circuit changes.
2. Lenz's Law: As an extension to Faraday's Law, Lenz's Law states that the emf induced will be such that the resulting induced current will oppose the change that produced it.
3. A combination of the above two laws is expressed in Maxwell's Third Equation

$$\mathbf{e} = -\frac{d\Phi}{dt} \quad (4.1)$$

where  $\mathbf{e}$  is the induced emf in *volts*, while  $\Phi$  is magnetic flux in *webers*.

4. Kirchoff's Voltage Law (KVL): The algebraic sum of the changes in potential encountered in a complete traversal of the circuit must be zero.
5. Kirchoff's Current Law (KCL): The algebraic sum of the currents at any junction in a circuit must be zero.

## 4.1 D.C. Motor

**Table 4.1 List of symbols used in this section**

<b>Variable/Parameter</b>	<b>Symbol</b>	<b>Units</b>
Permanent Magnet Stator Field of the Motor	$\mathbf{B}_m$	wb/m <sup>2</sup>
Armature Field of the Motor	$\mathbf{B}_a$	wb/m <sup>2</sup>
Armature Current in the Motor	$I_a$	A
Torque Constant of the Motor	$K_{t\_motor}$	N.m/A
Torque generated by the Motor	$T_m$	N.m
Flux linkage in Armature Coil due its own Current	$\Phi_a$	webers
Area Vector of Armature Coil (pointing in the same direction as $\mathbf{B}_a$ )	$\mathbf{A}$	m <sup>2</sup>
Armature Resistance	$R_a$	ohms
Armature Inductance	$L_a$	henry
Number of Armature Coils	$N$	-
Input Terminal Voltage to the Motor	$V_{in}$	V
Back emf generated in the Motor	$V_{backemf}$	V
Angular velocity of the Armature	$\omega$	rad/s
Back emf Constant	$K_{b\_motor}$	V.s/rad

A commonly encountered description for a DC motor is illustrated in the following circuit, with armature resistance and inductance modeled as lumped quantities.

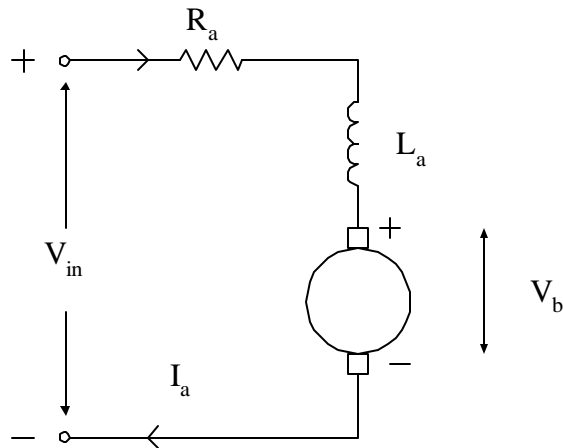


**Figure 4.1 Electrical Circuit for a D.C. Motor**

Applying KVL to the above circuit leads to the well-known DC motor electrical equation,

$$V_{in} - K_{b\_motor} \omega - L_a \frac{d I_a}{dt} = R_a I_a \quad (4.2)$$

To understand the significance of each term in the above equation, it is desirable to take a look at the derivation of this equation from a much more fundamental level. Consider the following physical model for a DC motor,

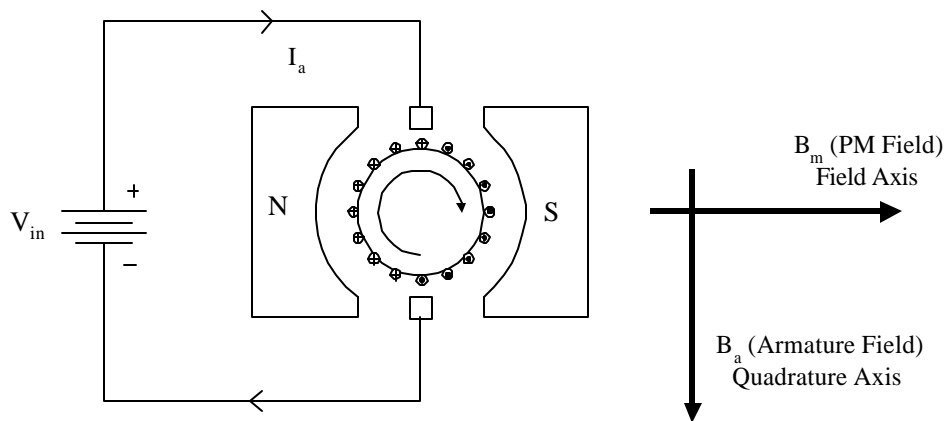


**Figure 4.2 Physical Model of a D.C. Motor**

The permanent magnet stator field ( $\mathbf{B}_m$ ), the direction of which is called the ‘field axis’, is fixed in space. The armature field ( $\mathbf{B}_a$ ), generated due to the armature current, is orientated in a direction called the ‘quadrature axis’. Despite the armature rotation, the quadrature axis retains its orientation in space due to commutation. If we assume a perfect commutation, then the armature field always remains perpendicular to the stator field. Repulsion between these two magnetic field vectors produces a clockwise torque on the rotor that is proportional to the product of  $\mathbf{B}_m$  and  $\mathbf{B}_a$ .  $\mathbf{B}_m$  remains constant and  $\mathbf{B}_a$  is linearly dependent on  $I_{\text{motor}}$ .

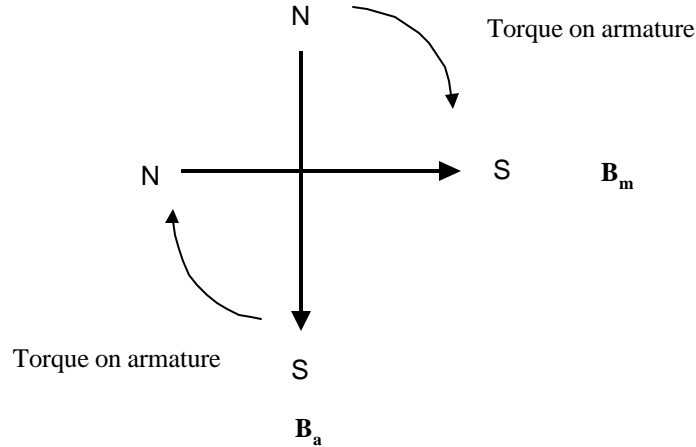


**Figure 4.3 Interaction between two magnetic fields**

Hence, the motor torque generated can be expressed as,

$$T_m = k \vec{B}_a \times \vec{B}_m = \vec{m} \times \vec{B}_m \quad (4.3)$$

where  $\vec{m}$  is the magnetic dipole moment resulting from the armature field, and is proportional to and in the same direction as  $\mathbf{B}_a$ .

$$\begin{aligned}
k \vec{B}_a &= \vec{m} \\
\vec{m} &= N I_a \vec{A} \quad (\text{by definition of magnetic dipole moment}) \\
\Rightarrow T_m &= N I_a \vec{A} \times \vec{B}_m \\
\Rightarrow T_m &= N A B_m I_a
\end{aligned} \tag{4.4}$$

Defining the motor torque constant  $K_{t\_motor} = N A B_m$ , we arrive at the following simple expression for motor torque

$$T_m = K_{t\_motor} I_a \tag{4.5}$$

Applying KVL and Ohm's Law, the governing electrical equation is expressed as,

$$V_{in} - V_{backemf} - N \frac{d\Phi_a}{dt} = R_a I_a \tag{4.6}$$

As is evident from the above equation, there are two effects that oppose  $V_{in}$ : a back emf that arises due to the armature motion in the stator field  $\mathbf{B}_m$ , and an induced emf due to the self-inductance of the armature coil. Both these effects are impeding effects, which is reflected by the negative sign associated with them (Lenz's Law). Also, using the following standard relationships,

$$\begin{aligned}
\Phi_a &= \vec{B}_a \cdot \vec{A} \\
N\Phi_a &= L_a I_a \\
V_{backemf} &= K_{b\_motor} \omega \quad (\text{generator effect, derieved in Section 4.2})
\end{aligned} \tag{4.7}$$

we can reduce equation (4.6) to,

$$V_{in} - K_{b\_motor} \omega - L_a \frac{d I_a}{dt} = R_a I_a \tag{4.8}$$

which is the same as equation (4.2). This is the commonly accepted model for an 'electromagnetically isolated' D.C. motor. Now we proceed to take a look at the model for D.C. tachometer.

## 4.2 D.C. Tachometer

**Table 4.2 List of symbols used in this section**

<b>Variable/Parameter</b>	<b>Symbol</b>	<b>Units</b>
Permanent Magnet Stator Field of the Tachometer	$\mathbf{B}_m$	wb/m <sup>2</sup>
Armature Field of the Tach	$\mathbf{B}_a$	wb/m <sup>2</sup>
Load Current drawn from the Tach	$I_L$	A
Torque Constant of the Tach	$K_{t\_tach}$	N.m/A
Retarding Torque generated by the Tachometer	$T_{tach}$	N.m
Flux linkage in the Tach Armature Coil due its own Current	$\Phi_a$	webers
Area Vector of Armature Coil (pointing in the same direction as $\mathbf{B}_a$ )	$\mathbf{A}$	m <sup>2</sup>
Armature Resistance	$R_a$	ohms
Armature Inductance	$L_a$	henry
Number of Armature Coils	$N$	-
Back emf generated in the Tach	$V_b$	V
Angular velocity of the Armature	$\omega$	rad/s
Generator Constant for the Tachometer	$K_{b\_tach}$	V.s/rad
Load Resistance	$R_L$	ohms

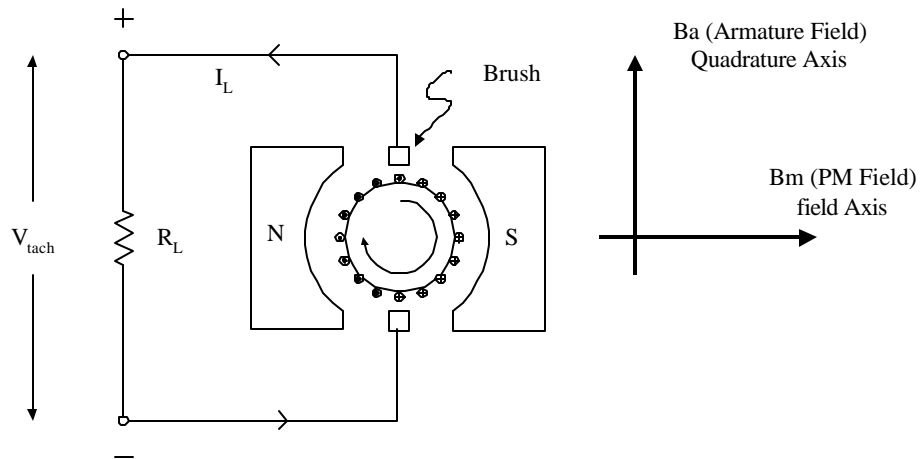


**Figure 4.4 Physical model of a D.C. tachometer**

In this case, a CW rotation of the rotor in the presence of the permanent magnet stator field  $\mathbf{B}_m$ , produces an emf of  $V_b$  across the armature terminals (Faraday's Law of Induction: Generator Effect).

Using Faraday's Law, we know that the emf induced in a conductor of length  $l$ , moving with a velocity  $v$ , in a uniform magnetic  $B$  field, is given by,

$$emf = l \vec{v} \times \vec{B} \quad (4.9)$$

It can be shown that for a coil rotating in a radially uniform stator field  $\mathbf{B}_m$ , the induced emf is given by,

$$\begin{aligned} V_b &= N 2l (\mathbf{w}r) B_m \\ \Rightarrow V_b &= N (2lr) B_m \mathbf{w} \\ \Rightarrow V_b &= N A B_m \mathbf{w} \end{aligned} \quad (4.10)$$

Defining the generator constant (or the tachometer constant) as  $K_{b\_tach} = N A B_m$ , leads us to the following simple relationship for the generator (or tachometer),

$$V_b = K_{b\_tach} \mathbf{w} \quad (4.11)$$

This induced emf causes a current  $I_L$  in the load resistor,  $R_L$ .  $I_L$  also flows through the tachometer armature, thus producing an armature field  $\mathbf{B}_a$  along the ‘quadrature axis’. Once again due to commutation, the orientation of the armature field always remains perpendicular to the stator field and hence is fixed in space. This current also produces a retarding torque on the tachometer rotor, which as earlier can be derived to be the following,

$$T_{tach} = K_{t\_tach} I_L \quad (4.12)$$

KVL and Ohm’s Law for the above tachometer circuit leads to,

$$V_b - N \frac{d \Phi_a}{dt} = (R_a + R_L) I_L \quad (4.13)$$

Using equations (4.11) and (4.7), this equation further reduces to,

$$K_{b\_tach} \mathbf{w} - L_a \frac{d I_L}{dt} = (R_a + R_L) I_L \quad (4.14)$$

The first term on the LHS represents the voltage induced across the armature due to its motion in the permanent magnet field  $\mathbf{B}_m$ . Consequently, since the circuit is closed by means of the external resistance  $R_L$ , a current  $I_L$  flows through the circuit. The self-inductance of the coil tries to oppose the emf that causes  $I_L$ , hence the negative sign associated with the second term (Lenz’s Law). The terminal voltage as seen by the resistor  $R_L$  is given by,

$$V_{tach} = R_L I_L = K_{b\_tach} \mathbf{w} - L_a \frac{d I_L}{dt} - R_a I_L \quad (4.15)$$

If  $R_L$  is extremely large, then the current drawn from the tachometer is negligible and the above expression is reduced to,

$$V_{tach} = K_{b\_tach} \mathbf{w} \quad (4.16)$$

This is the model for an ‘electromagnetically isolated’ tachometer that we encounter in all textbooks and references. Now we proceed to investigate how this changes when a DC tachometer is placed close to a DC motor.

### 4.3 Coupled D.C. Motor-Tachometer System

**Table 4.3 List of symbols used in this section  
(units are the same as earlier)**

<b>Variable/Parameter</b>	<b>for Motor</b>	<b>for Tach</b>
Permanent Magnet Stator Field	$\mathbf{B}_{m1}$	$\mathbf{B}_{m2}$
Armature Field	$\mathbf{B}_{a1}$	$\mathbf{B}_{a2}$
Armature Current	$I_1$	$I_2$
Torque Constant	$K_{t\_motor}$	$K_{t\_tach}$
Torque generated	$T_m$	$T_{tach}$
Flux linkage in Armature Coil due its own Current	$\Phi_1$	$\Phi_2$
Area Vector of Armature Coil (pointing in the same direction as armature field)	$\mathbf{A}_1$	$\mathbf{A}_2$
Armature Resistance	$R_1$	$R_2$
Armature Inductance	$L_1$	$L_2$
Number of Armature Coils	$N_1$	$N_2$
Angular velocity of the Armature	$\omega_m$	$\omega_{tach}$
Back emf Constant / Generator Constant	$K_{b\_motor}$	$K_{b\_tach}$

All the preceding discussions were carried out assuming that both devices are electrically and magnetically isolated. Now consider a mechanically coupled motor-tachometer system like the one shown Figure 4.5(a). The two armature rotors are connected by a shaft of finite stiffness. In general, there can be an angular offset between the motor stator field and the tachometer stator field, say,  $\alpha$  in this case.

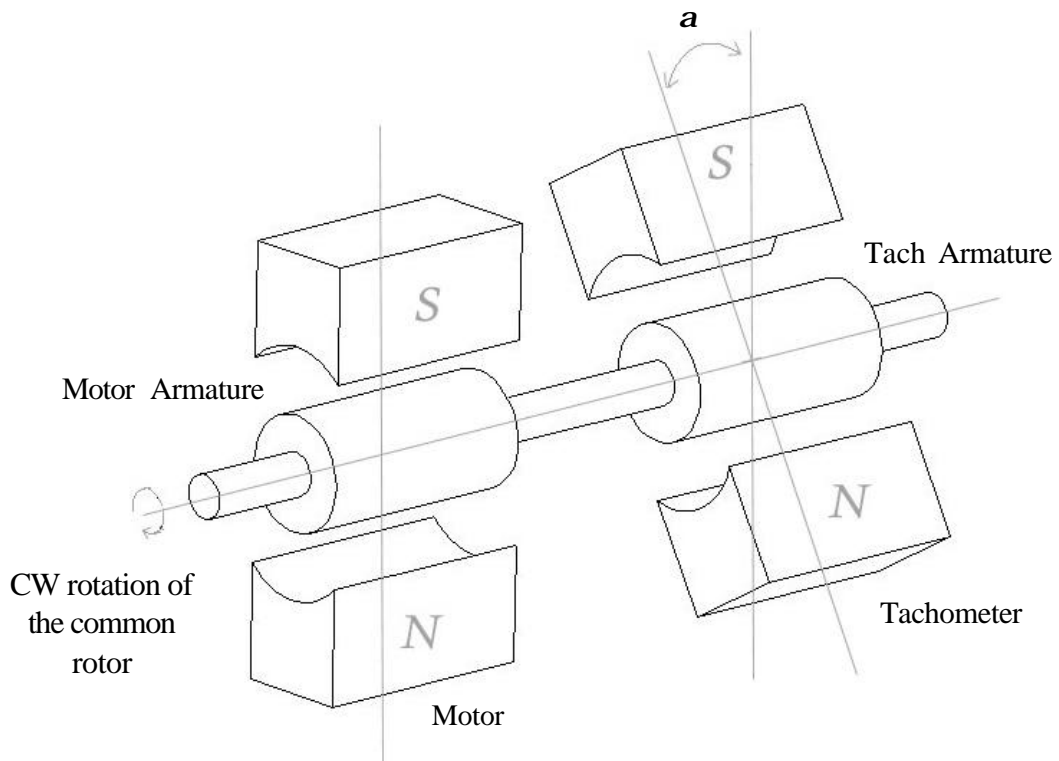
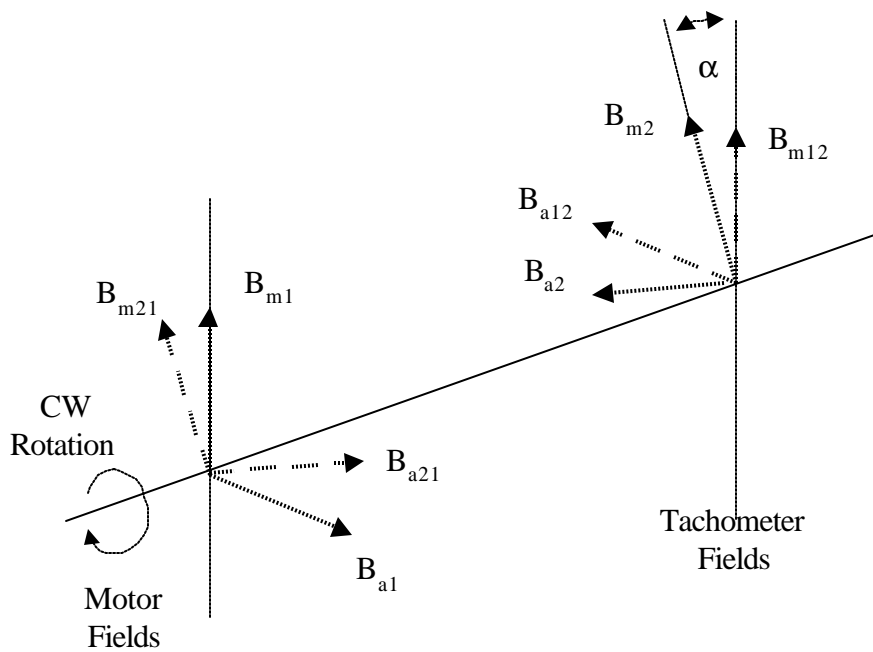


**Figure 4.5 (a) Angular orientations of the Motor and Tachometer permanent magnets (b) Motor and Tachometer Fields**



We notice that the armature field of the motor produces a flux linkage in the tachometer winding and similarly the armature field of the tachometer produces a certain flux linkage in the motor winding, which in effect leads to mutual inductance between the two coils. This effect is better understood from Figure 4.5(b), which shows all the fields that play a role in the motor-tachometer interaction.

In the Figure 4.5(b), we indicate the respective stator fields,  $\mathbf{B}_{m1}$  and  $\mathbf{B}_{m2}$ , and the armature fields,  $\mathbf{B}_{a1}$  and  $\mathbf{B}_{a2}$ , of the motor and tachometer. Directions of  $\mathbf{B}_{m1}$  and  $\mathbf{B}_{m2}$  are defined by the orientation of permanent magnet stators. For clockwise rotation of the rotors, directions of  $\mathbf{B}_{a1}$  and  $\mathbf{B}_{a2}$  are obtained from Figures 4.2 and 4.3 respectively. Since the two devices are not magnetically insulated, the tachometer armature (coil 2) sees a weak field,  $\mathbf{B}_{a12}$ , due to the motor armature current. Thus,  $\mathbf{B}_{a12}$  is defined as the magnetic field due to motor armature current ( $I_1$ ) experienced by the tachometer armature (coil 2). Obviously,  $\mathbf{B}_{a12}$  is in the same plane as  $\mathbf{B}_{a1}$ , but is opposite in direction. The tachometer also experiences the effect of the permanent magnets of the motor. This appears in the form of a weak field  $\mathbf{B}_{m12}$ , resulting from the leakage flux of the permanent magnets of the motor.  $\mathbf{B}_{m12}$  is in the same direction as  $\mathbf{B}_{m1}$ . We summarize all these fields in the following vector diagram for the tachometer, derived from Figure 4.5(b).

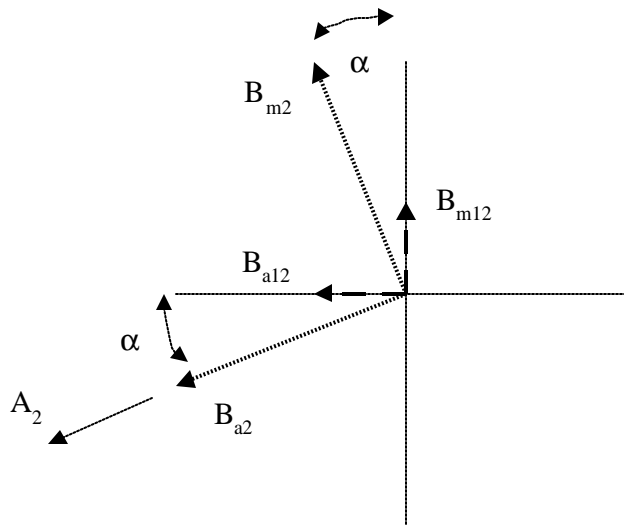


**Figure 4.6(a) Magnetic Fields present in the Tachometer**

In a very similar way, the motor winding (coil 1) experiences a magnetic field,  $\mathbf{B}_{a21}$ , due to the current  $i_2$  in the tachometer armature (coil 2). Once again, the direction of  $\mathbf{B}_{a21}$  is opposite to the direction of  $\mathbf{B}_{a2}$ . There is also an effect of the tachometer permanent magnets that is seen by the motor in the form of a weak field,  $\mathbf{B}_{m21}$ , acting in the direction of  $\mathbf{B}_{m1}$ . As discussed in Sections 4.1 and 4.2, these directions remain fixed in space. From Figure 4.5(b), all the magnetic fields that appear in the motor are shown in the following figure.

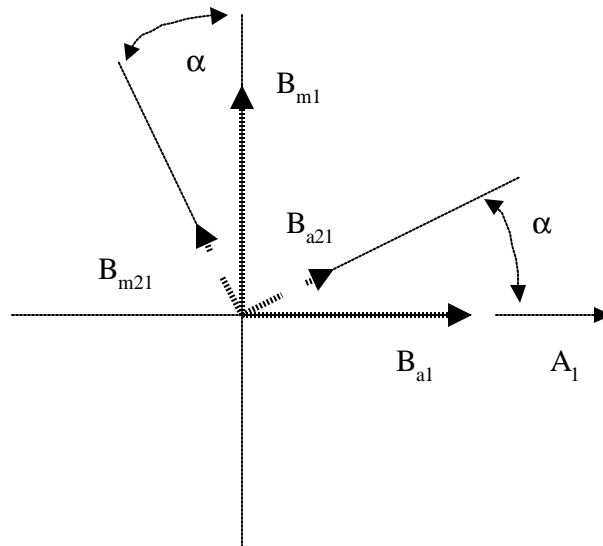


**Figure 4.6(b) Magnetic Fields present in the Motor**

It is worth-mentioning here that the effect of  $\mathbf{B}_{m12}$  on the tachometer equations is negligible. It does not lead to any dynamic effects; it only changes the stator field that the tachometer armature rotates in, by a very small amount. This in turn causes a slight variation in the torque constant and the generator/tachometer constant. Nevertheless, the governing relationships given by equations (4.11) and (4.12) remain unaltered. Similarly,  $\mathbf{B}_{m21}$  is of little consequence in the motor equations, except for causing a small change in the torque constant and back-emf constant. For the case of the motor, equation (4.5) is still valid.

The presence of the armature fields  $B_{a12}$  and  $B_{a21}$  lead to mutual inductance between the two coils. Let us look at this transformer effect between the two armature coils: motor armature (coil1) and tachometer armature (coil 2), in terms of flux linkages. The magnitudes of the armature fields are linearly dependent on the respective armature currents. Therefore the following holds,

$$\begin{aligned}
 B_{a1} &= k_1 I_1 \\
 B_{a21} &= k_{21} I_2 \\
 B_{a2} &= k_2 I_2 \\
 B_{a12} &= k_{12} I_1
 \end{aligned}
 \tag{4.17}$$

where  $k_1$ ,  $k_2$ ,  $k_{12}$  and  $k_{21}$  are constants.

In this case we have a weak transformer effect unlike that in an ideal transformer. An ideal transformer has the following properties

1. Winding resistances are negligible
2. All fluxes are confined to the core and link both windings. There are no leakage fluxes present and core losses are assumed to be negligible.
3. Permeability of core is infinite. Therefore, the excitation current required to establish flux in the core is negligible.

When these properties are closely satisfied, then the following relationships hold,

$$\begin{aligned}
 \frac{V_1}{V_2} &= \frac{N_1}{N_2} \\
 \frac{i_1}{i_2} &= \frac{N_2}{N_1}
 \end{aligned}
 \tag{4.18}$$

Referring to Figure 4.7, which illustrates the case at hand, the situation is very different from an ideal transformer, since none of the above requirements are met. There is no core between the two coils, the permeability of air is very low, and most part of the flux linked with each coil is leakage flux and mutual flux is small. Hence the relationships (4.18) do not hold in this case.

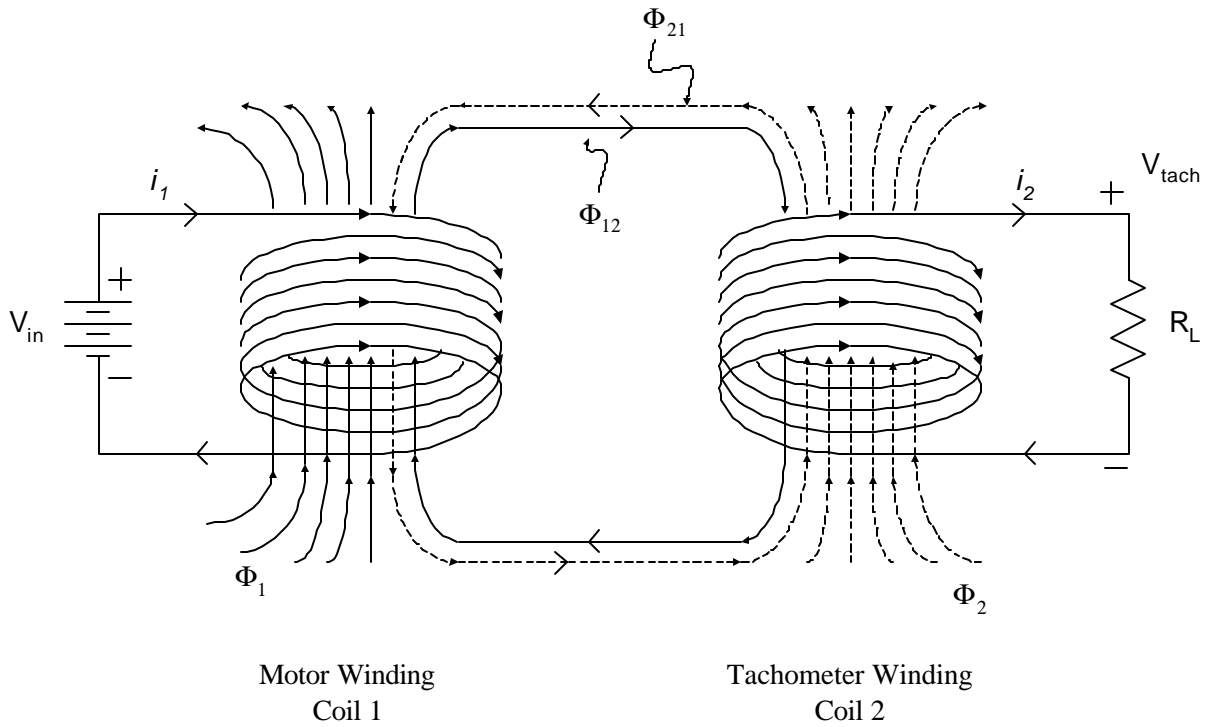


**Figure 4.7 Transformer effect between the motor armature coil and tachometer armature coil**

In the above figure,

$\Phi_1$  is the flux linkage in coil 1 due to current in coil 1 ( $I_1$ )

$\Phi_{21}$  is the flux linkage in coil 1 due to current in coil 2 ( $I_2$ )

$\Phi_2$  is the flux linkage in coil 2 due to current in coil 2 ( $I_2$ )

$\Phi_{12}$  is the flux linkage in coil 2 due to current in coil 1 ( $I_1$ )

Then, by referring to Figures 4.6 (a) and (b), and expressions (4.17), we conclude that

$$\Phi_1 = \vec{B}_{a1} \cdot \vec{A}_1 = (k_1 I_1) A_1 \quad (4.19)$$

$$\Phi_2 = \vec{B}_{a2} \cdot \vec{A}_2 = (k_2 I_2) A_2 \quad (4.20)$$

$$\Phi_{21} = \vec{B}_{a21} \cdot \vec{A}_1 = (k_{21} I_2) A_1 \cos(\mathbf{a}) \quad (4.21)$$

$$\Phi_{12} = \vec{B}_{a12} \cdot \vec{A}_2 = (k_{12} I_1) A_2 \cos(\mathbf{a}) \quad (4.22)$$

Consequently, the resultant flux linkage in motor armature (coil1) =  $\Phi_1 + \Phi_{21}$

and, the resultant flux linkage in tachometer armature (coil2) =  $\Phi_2 + \Phi_{12}$

Applying KVL and Ohm's Law to the electrical circuit comprising coil 1, i.e. the motor armature, we get

$$V_{in} - V_{backemf} - N_1 \frac{d(\Phi_1 + \Phi_{21})}{dt} = R_1 I_1 \quad (4.23)$$

This is similar to equation (4.6) in Section 4.1, with the only difference being that, in equation (4.6) the mutual flux term was missing. The significance and sign of each term in the above equation has been explained in Section 4.1.

The application of KVL and Ohm's Law to the electrical circuit containing the tachometer armature (coil 2) in Figure 4.7, leads to

$$V_b - N_2 \frac{d(\Phi_2 + \Phi_{12})}{dt} = (R_2 + R_L) I_2 \quad (4.24)$$

Once again, this is similar to equation (4.13) derived in Section 4.2. Equation (4.24) includes a mutual flux term which equation (4.13) was lacking. The significance and sign of each term in the above equation has been explained in Section 4.2.

Using equations (4.19)-(4.22), we are now in a position to define inductances,

$$N_1 \Phi_1 = N_1 (K_1 I_1) A_1 \triangleq L_1 I_1 \quad (4.25)$$

$$N_2 \Phi_2 = N_2 (K_2 I_2) A_2 \triangleq L_2 I_2 \quad (4.26)$$

$$N_1 \Phi_{21} = N_1 (K_{21} I_2) A_1 \cos(\mathbf{a}) \triangleq M_{21} I_2 \cos(\mathbf{a}) \quad (4.27)$$

$$N_2 \Phi_{12} = N_2 (K_{12} I_1) A_2 \cos(\mathbf{a}) \triangleq M_{12} I_1 \cos(\mathbf{a}) \quad (4.28)$$

$$M_{12} = M_{21} \quad (4.29)$$

$L_1$  and  $L_2$  are the self-inductance values for the motor and tachometer coils respectively.  $M_{12}$  ( =  $M_{21}$  ) is the mutual inductance value between the motor and tachometer coils, when  $\alpha = 0^\circ$  .

Furthermore, using the previously derived expressions,

$$V_{backemf} = K_{b\_motor} \mathbf{w}_m$$

$$V_b = K_{b\_tach} \mathbf{w}_{tach}$$

and results (4.25) - (4.28), the motor equation (4.23) reduces to,

$$V_{in} - K_{b\_motor} \mathbf{w}_m - L_1 \frac{d I_1}{dt} - M_{21} \cos(\mathbf{a}) \frac{d I_2}{dt} = R_1 I_1 \quad (4.30)$$

and the tachometer equation (4.24) reduces to,

$$K_{b\_tach} \mathbf{w}_{tach} - L_2 \frac{d I_2}{dt} - M_{12} \cos(\mathbf{a}) \frac{d I_1}{dt} = (R_2 + R_L) I_2 \quad (4.31)$$

The tachometer terminal voltage measured by an external device is  $R_L I_2$ ,

$$\therefore V_{tach} = R_L I_2 = K_{b\_tach} \mathbf{w}_{tach} - L_2 \frac{d I_2}{dt} - M_{12} \cos(\mathbf{a}) \frac{d I_1}{dt} - R_2 I_2 \quad (4.32)$$

This is the enhanced tachometer model that includes the effect of mutual inductance between motor and tachometer armatures, which is ignored in the conventional model. Torque models for the motor and tachometer are relatively simple. The retarding torque produced by the tachometer is given by,

$$T_{tach} = K_{t\_tach} I_2 \quad (4.33)$$

and the torque generated by the motor can be expressed as,

$$T_m = K_{t\_motor} I_1 \quad (4.34)$$

The derivation of these relationships has been covered in Section 4.1. Thus, the net torque output by the motor-tachometer assembly is,

$$T_{out} = K_{t\_motor} I_1 - K_{t\_tach} I_2 \quad (4.35)$$

Equations (4.30) through (4.35) are the final results of this derivation. The signs associated with each term in these equations are very important, as they can significantly effect the system dynamics. At this stage we can consider making some simplifications. A pragmatic observation is that  $I_2$  (load current) is much smaller than  $I_1$  (motor current). In fact, if  $R_L$ , the input impedance of the voltage-measuring device (e.g. SigLab) is high, which it is in this case ( $\sim 1$  Mohm), then the current drawn from the tachometer is almost negligible. We can therefore eliminate terms containing  $I_2$ , wherever it occurs in equations (4.30) - (4.35), which leads to some simplification. At this point however, we shall retain the term ' $-R_2 I_2$ ' in the  $V_{\text{tach}}$  expression from equation (4.32). This is done to resolve a singularity at a later stage. Since this term constitutes a damping term, the sign associated with it is very important in determining the phase change at zero and pole frequencies. In the absence of this term, the model sees a singularity and arbitrarily assigns either a  $+180^\circ$  or  $-180^\circ$  phase change. A damping term, however small (even negligible), resolves this singularity and determines whether this phase change has to be  $+180^\circ$  or  $-180^\circ$ , depending upon the sign associated with this damping term. Thus, this term is retained only to predict the phase plot in frequency response. It has no effect on the magnitude plot whatsoever.

A final observation is made regarding the ' $-R_2 I_2$ ' term. Had the transformer effect been an ideal one, the relationship (4.18) would hold, i.e.,  $I_2 = (N_1/N_2) I_1$ . In the present case, this is not true, since the transformer effect is a weak one. Nevertheless,  $I_2$  may be weakly related to  $I_1$  by some empirical constant. Based on this argument, we suggest that ' $R_2 I_2$ ' may be replaced by ' $K_r I_1$ ' where  $K_r$  is an experimentally determined empirical constant. The validity of this empirical conjecture, though questionable at this stage, shall be confirmed experimental measurements. Experimental verification is covered in the following section.

Implementing these discussions, the motor-tachometer equations reduce to,

Motor Equation:  $V_{in} - K_{b\_motor} \mathbf{w}_m - L_1 \frac{d I_1}{dt} = R_1 I_1$

Tachometer Equation:  $V_{tach} = K_{b\_tach} \mathbf{w}_{tach} - M_{12} \cos(\mathbf{a}) \frac{d I_1}{dt} - R_2 I_2$  (4.36)

Torque Equation:  $T_{out} = K_{t\_motor} I_1$

Comparing these results with the previous results, we notice that the motor model and the torque expression remain the same, while the tachometer model has additional terms in it, that were missing in the conventional model.

Rewriting the tachometer equation,

$$V_{tach} = K_{b\_tach} \mathbf{w}_{tach} + K_m \frac{d I_1}{dt} - K_r I_1$$

$K_m \triangleq -M_{12} \cos(\mathbf{a})$  (magnetic coupling constant) (4.37)

$K_r \triangleq R_2 (I_2 / I_1)$  (loading effect constant)

This is final form of the enhanced tachometer model. Note that since the tachometer is magnetically coupled to the motor, the motor current influences the tachometer terminal voltage despite the fact that the two are electrically insulated. This model reduces to the conventional model, given by equation (4.16), if the magnetic coupling constant  $K_m = 0$ , and the loading effect constant  $K_r = 0$ . These two constants are easily determined experimentally, as shall be described in the next section.  $K_r$  is always positive, while  $K_m$  may be positive or negative depending on the angle  $\alpha$ .

## 5. EXPERIMENTAL VERIFICATION OF THE PROPOSED MODEL

**Table 5.1 List of symbols used in this section**

Variable	Symbol
Motor angular position	$\theta_m$
Tachometer angular position	$\theta_t$
Motor current	$i_m$
Motor torque	$T_m$
Tachometer voltage	$V_{tach}$

Parameter	Symbol	Value	Source
Motor armature inertia	$J_m$	43.77e-6 kg-m <sup>2</sup>	Manf. Specs.
Tachometer armature inertia	$J_t$	11.35e-6 kg-m <sup>2</sup>	Manf. Specs.
Motor-Tachometer shaft stiffness	$K$	1763.2 N-m/rad	Parameter ID
Motor torque constant	$K_t$	8.33e-2 N-m/A	Manf. Specs.
Tachometer constant	$K_{tach}$	0.1377 V/rad/s	Manf. Specs.
Magnetic Coupling constant	$K_m$	8.8852e-5 Henry	Parameter ID
Loading effect constant	$K_r$	2.6656e-2 Ohms	Parameter ID

We now incorporate the tachometer model obtained in Section 4.3, in the analysis for the motor-tachometer system that we studied earlier in Section 3. The transfer function of mechanical system from equation (3.1) remains unchanged,

$$\frac{q_t}{T_m} = \frac{K}{s^2 [J_t J_m s^2 + K(J_t + J_m)]} \quad (5.1)$$

DC motor operating in current mode can also be modeled as earlier,

$$\begin{aligned} T_m &= K_t i_m \\ i_m &= K_{amp} V_{in} \\ T_m &= K_{amp} K_t V_{in} \end{aligned} \quad (5.2)$$

Based on Section 4.3, the tachometer output is now expressed as,

$$V_{tach} = K_{tach} \dot{\mathbf{q}}_t + K_m (di_m / dt) - K_r i_m \quad (5.3)$$

The expressions (5.1)–(5.3) yield the following overall transfer function for the unloaded motor-tachometer system,

$$\frac{V_{tach}}{V_{in}} = \frac{K_{amp} [K_m (den) s^2 - K_r (den) s + K_t K_{tach} K]}{(den) s} \quad (5.4)$$

$$(den) \triangleq [J_t J_m s^2 + K (J_t + J_m)]$$

This analytically obtained transfer function for the tachometer-motor system is used to generate the frequency response plots in MATLAB. These plots are then compared to the experimentally obtained plots

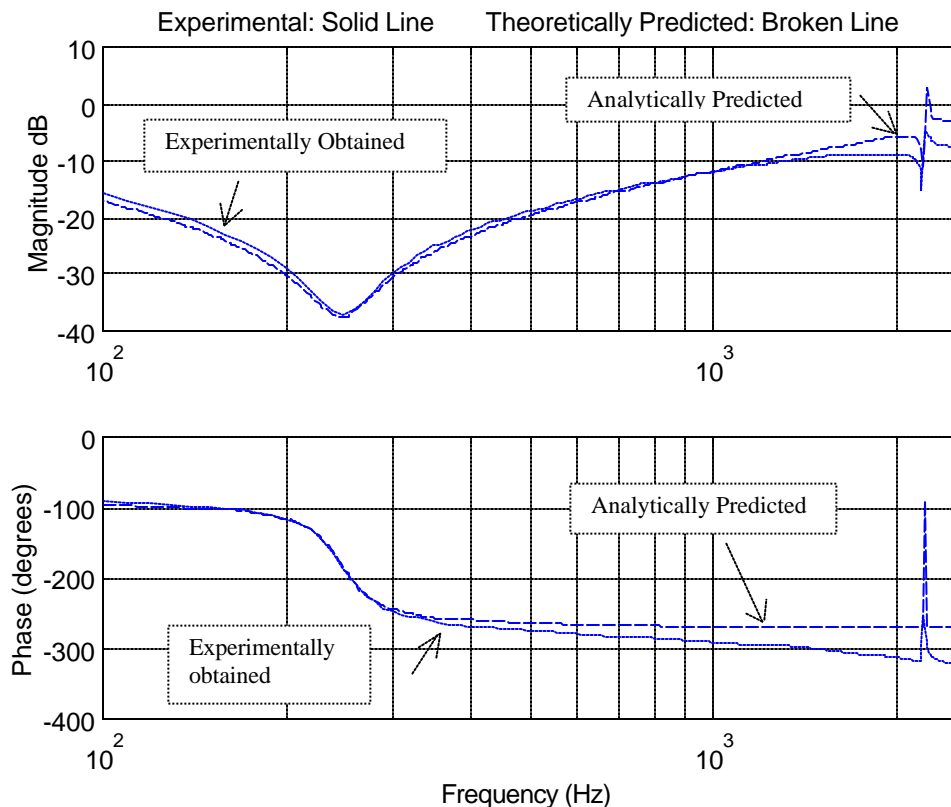


**Figure 5.1  $V_{tach}/V_{in}$  : Comparison of analytically predicted and experimentally obtained frequency response plots for the motor-tachometer system**

Some interesting observations made from the above comparison are listed here:

1. The new model predicts the experimental observation even for the high frequency range very accurately. The analytical plot does indicate the presence of two complex-conjugate zeros that are observed in the experimental plots.
2. Looking at the system transfer function given by equation (5.4), we can now explain the presence of the additional zeros. It is evident that a positive  $K_m$  leads to complex conjugate zero pairs in the system. Clearly, these zeros will disappear for  $K_m=0$ . In this particular case we have two complex conjugate zero pairs which is one more than the number of complex conjugate pole pairs.
3. The presence of  $K_r$  with a negative sign explains why the phase drops by  $180^\circ$  at the first zero frequency. The loading effect pushes the first complex-conjugate pole pair to the right side of the imaginary axis on the  $s$ -plane. The importance of the negative sign associated with  $K_r$  becomes evident here, which is why signs were dealt with care during the derivation of the tachometer model.
4. Although the conventional model predicted the system poles accurately, it failed to explain the presence of system zeros. The new model addresses this inconsistency very well.

Once the new tachometer model is experimentally confirmed, the results of the above experimental plots are then used to back-calculate the exact values of the parameters  $K$  (shaft stiffness),  $K_m$  (magnetic coupling constant) and  $K_r$  (loading effect constant). In Figure 5.1, the first zero frequency is 247 Hz, and the second zero frequency is 2200 Hz. The pole next to the second zero is at 2230 Hz. Equating the predicted pole frequency expression to experimentally obtained frequency, we get  $K=1763.2$  N-m/rad. Equating the predicted zero frequency expressions to experimentally obtained zero frequencies, we get  $K_m=8.62565e-5$  Henry. From the experimental plot, the damping at the first pole is estimated to be  $\zeta=0.098$ . Equating this to the theoretically predicted expression for damping, we get  $K_r=2.6656e-2$  Ohms. Note that  $K_m$  and  $K_r$  are very small numbers.

## 5.1 Discussion on the proposed tachometer model

We thus see that for an accurate prediction of experimental results, the simple ‘gain’ model for tachometer is not sufficient. An accurate tachometer model is developed in the preceding sections. We now state some observations/conclusions based on the new model:

1. The most noticeable enhancement in the new tachometer model is the presence of a magnetic coupling constant,  $K_m$ . If  $K_m$  were made zero, which happens when  $\alpha = 90^\circ$ , or when the two coils are magnetically insulated, i.e. the mutual inductance  $M_{12} = 0$ , we see that the transformer coupling vanishes. Taking a closer look at the magnetic coupling factor  $K_m$ ,

$$K_m = -M_{12} \cos \alpha$$

where  $\alpha$  is the angular misalignment between motor field and tachometer field, and  $M_{12}$  is the mutual inductance between motor winding and tachometer winding for  $\alpha=0$ .  $K_m$  is a geometry dependent parameter and is best determined experimentally. This parameter has a very significant influence on tachometer dynamics, as it determines the strength and sign of coupling. For example,

if  $\alpha = \pm 90^\circ$ , the effect of coupling is annulled,

if  $\alpha = 0^\circ$ ,  $K_m$  is maximum negative, which leads to real zeros and thus a non-minimal phase system,

if  $\alpha = 180^\circ$ ,  $K_m$  is maximum positive, and this leads to complex-conjugate zeros lying close to the complex conjugate poles of the system.

Whatever this angle  $\alpha$  is, it has a significant influence on system poles and zeros, and hence the design of a controller.

2. Because of the magnetic coupling term, the denominator of the system transfer function finds a place in the numerator, as is evident in equation (5.4). Hence the additional zeros that appear are strongly dependent on the system poles. If all poles

- are complex-conjugate pairs, and if  $K_m$  is positive, then all the resulting zeros are also complex conjugate pairs, and the number of these zero pairs is one greater than the number of complex conjugate pole pairs (excluding the poles at the origin).
3. The other important parameter that appears in proposed tachometer expression is the empirical constant  $K_r$ , which is always positive. Once again, since  $K_r$  is dependent on the experimental set-up, it is best obtained experimentally. If the additional zeros are complex conjugate, the negative sign associated with  $K_r$  pushes them slightly into the right half of s-plane. This phenomenon helps in predicting the phase change at the zero frequencies in the phase vs. frequency plots.
  4. The significance of the signs associated with  $K_r$  and  $K_m$  is now evident since these signs dictate the nature and location of the additional zeros. This is the reason why the importance of signs was emphasized during the derivation of the tachometer model.

## 6. TYPICAL APPLICATION: MOTION CONTROL IN PRESENCE OF SHAFT COMPLIANCE

**Table 6.1 List of symbols used in this section**

Variable	Symbol
Motor angular position	$\theta_m$
Tachometer angular position	$\theta_t$
Inertia 1 angular position	$\theta_1$
Inertia 2 angular position	$\theta_2$
Motor current	$i_m$
Motor torque	$T_m$
Tachometer voltage	$V_{tach}$

Parameter	Symbol	Value
Motor armature inertia	$J_m$	43.77e-6 kg-m <sup>2</sup>
Tachometer armature inertia	$J_t$	11.35e-6 kg-m <sup>2</sup>
Inertia 1	$J_1$	18.77e-6 kg-m <sup>2</sup>
Inertia 2	$J_2$	18.77e-6 kg-m <sup>2</sup>
Motor-Tachometer shaft stiffness	$K$	1763 N-m/rad
Torsional stiffness of Shaft 1	$K_{shaft1}$	623 N-m/rad
Torsional stiffness of Shaft 2	$K_{shaft2}$	1063 N-m/rad
Torsional stiffness of coupling	$K_{coupling}$	1500N-m/rad
Effective torsional stiffness of Shaft 1, Shaft2 and coupling (in series)	$K_1$	311 N-m/rad
Torsional stiffness of Shaft 3	$K_2$	249 N-m/rad
Motor torque constant	$K_t$	8.33e-2 N-m/A
Tachometer constant	$K_{tach}$	0.1377 V/rad/s
Magnetic Coupling constant	$K_m$	8.8852e-5 Henry
Loading effect constant	$K_r$	2.6656e-2 Ohms
Voltage to current amplification	$K_{amp}$	0.5 A/V

We now consider a typical problem in DC motor motion control using tachometer feedback. The integrated motor-tachometer assembly described in Section 2 is used. The motor shaft is now connected to a load by means of a flexible coupling of known stiffness. Furthermore the load is in the form of two inertia's connected by a shaft. Thus the system has multiple flexible elements.

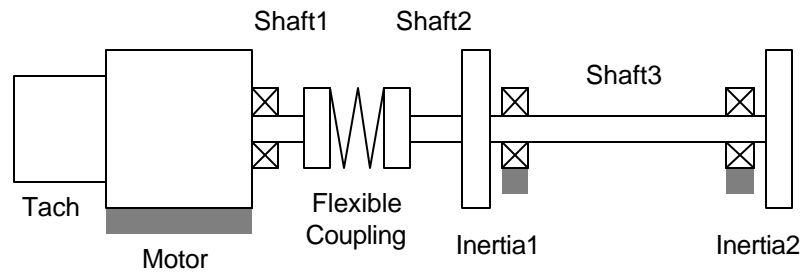


**Figure 6.1 Motor-tachometer-load System**

A lumped parameter model is used to describe the above system, with the assumption that dissipation terms (i.e. Coulomb friction, viscous damping and material damping) hardly influence the existence of system poles and zeros. As was discussed in Section 3, the purpose of the present investigation is to identify the poles and zeros of the overall system that arise due to the mechanical and electromagnetic characteristics of the system. From a frequency response perspective, mechanical damping does not govern the existence of these poles and zeros. It only tends to reduce their intensity as was illustrated in Figure 3.2. A more rigorous distributed parameter model with all dissipation terms included can be used to get a much more exact match between the zero and pole locations in the experimental and predicted plots. We do not use such a model here because the simple lumped parameter model with no dissipation assumption is sufficient to capture all the prominent attributes that are noticed in the experimental results. Our objective here is

to show the significant extent by which the new model changes the analytical predictions and indeed brings them very close to the experimental observations.

A physical model of the above system is shown below,

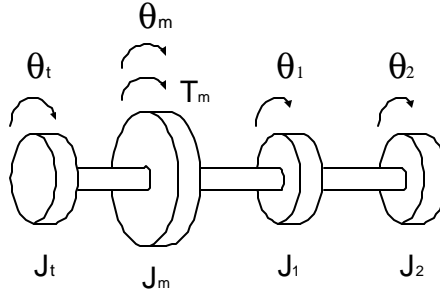


**Figure 6.2 Physical Model of the motor-tachometer-load system**

Drawing free-body diagrams for each of the four inertias and applying Newton's II Law, we arrive at the following transfer function for mechanical system,

$$\frac{\mathbf{q}_t}{T_m} = \frac{[num]}{s^2 \cdot [den]} \quad (6.1)$$

where,

$$\begin{aligned} [num] &= K [J_1 J_2 s^4 + (J_1 K_2 + J_2 K_1 + J_2 K_2) s^2 + K_1 K_2] \\ [den] &= s^6 [J_t J_m J_1 J_2] + \\ & s^4 [K_2 J_t J_m J_1 + K_1 J_t J_m J_2 + K_2 J_t J_m J_2 + \\ & K J_m J_1 J_2 + K J_t J_1 J_2 + K_1 K_t J_1 J_2] + \\ & s^2 [K_1 K_2 J_t J_m + K K_2 J_1 J_m + K K_1 J_2 J_m \\ & K K_2 J_2 J_m + K K_2 J_t J_1 + K K_1 J_t J_2 \\ & K K_2 J_t J_2 + K_1 K_2 J_t J_1 + K K_1 J_1 J_2 + K_1 K_2 J_1 J_2] \\ & + [K K_1 K_2 (J_t + J_m + J_1 + J_2)] \end{aligned} \quad (6.2)$$

The motor model is same as earlier,

$$\begin{aligned}
T_m &= K_t i_m \\
i_m &= K_{amp} V_{in} \\
T_m &= K_{amp} K_t V_{in}
\end{aligned} \tag{6.3}$$

The new tachometer model is given by equation (4.37),

$$V_{tach} = K_{tach} \dot{q}_t + K_m (di_m / dt) - K_r i_m \tag{6.4}$$

All these expressions (6.1)-(6.4) lead to the following overall system transfer function,

$$\frac{V_{tach}}{V_{in}} = \frac{K_{amp} [K_m s^2 (den) - K_r s (den) + K_t K_{tach} (num)]}{s (den)} \tag{6.5}$$

On the other hand, if we were to obtain the system transfer function using the conventional tachometer model, given by equation (4.16), we get the following

$$\frac{V_{tach}}{V_{in}} = \frac{K_{amp} K_t K_{tach} (num)}{s (den)} \tag{6.6}$$

Comparing the two transfer functions (6.5) and (6.6), it is clear that the new model captures some dynamics that is missing in the old model. Note that, in (6.5) if  $K_r = K_m = 0$ , then (6.5) reduces to (6.6).

Next we perform a sine-sweep experiment on the actual system to obtain its frequency response experimentally. We compare the experimentally obtained frequency plots with those predicted by the two models. Figure 6.3 presents a comparison of the experimental frequency plots with those predicted by the old model, expression (6.6). Figure 6.4 presents a comparison of the experimental results with the predictions of the new model, expression (6.5)

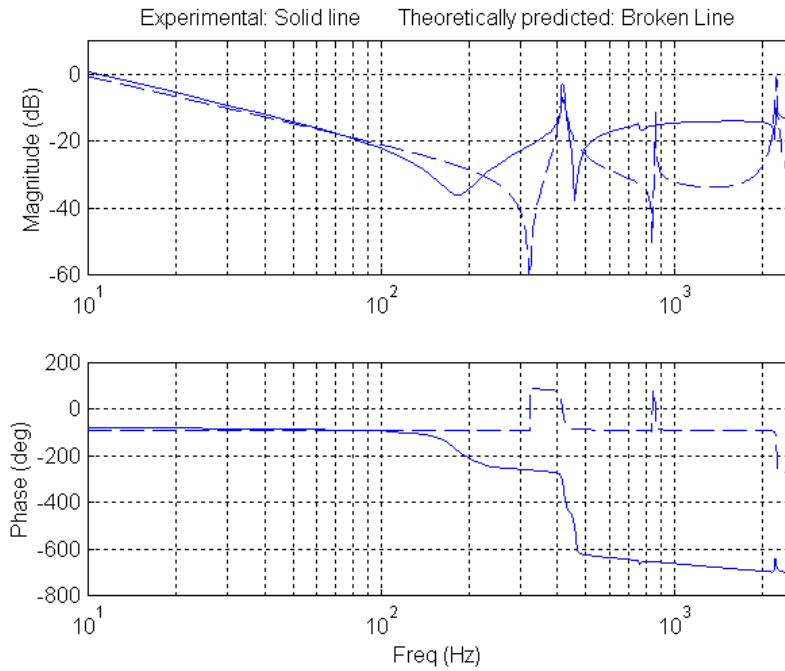


**Figure 6.3  $V_{tach}/V_{in}$  : Comparison of experimental frequency response and predicted frequency response using conventional model**

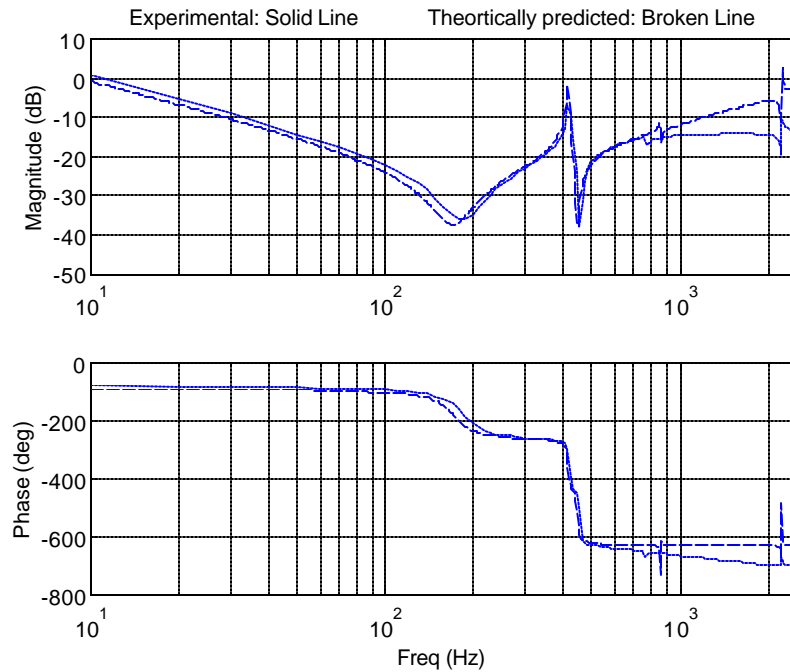


**Figure 6.4  $V_{tach}/V_{in}$  : Comparison of experimental frequency response and predicted frequency response using proposed model**

**Table 6.2 Comparison of experimentally observed and theoretically predicted (using the proposed model) zero and pole frequencies**

complex conjugate pair	Experimental	Theoretical
Zero	178 Hz	170 Hz
Pole	420 Hz	416 Hz
Zero	455 Hz	449 Hz
Pole	762 Hz	860 Hz
Zero	782 Hz	862 Hz
Zero	2200 Hz	2217 Hz
Pole	2230 Hz	2231 Hz

From the above comparison plots, we make the following observations

1. The analysis based on the conventional model completely fails to predict the experimental results at frequencies higher than 100 Hz. On the other hand the new model performs extremely well in explaining the experimental observation
2. The conventional model predicts only two complex conjugate zero pairs while the experimental results indicate that the system has four complex-conjugate zeros pairs, (one more in number than the complex conjugate pole pairs). The new model is able to successfully predict all these four complex conjugate zero pairs.
3. We also notice that the analysis based on conventional model successfully predicts the system poles but not the zeros.

Thus the overall system model, with the new tachometer model incorporated, can be now used for System Identification and Control System Design. We can conduct an experiment similar to the one described above for the purpose of parameter identification. Each of the complex conjugate pole pairs in the system transfer function represents a resonance mode of the system arising from the flexible elements (e.g., compliant shaft, flexible coupling etc.). Thus if the stiffness of some flexible member is unknown and can't be measure directly, it can be easily back-calculated from the pole frequency

locations obtained from experimental data and an accurate knowledge of the complete system model. This was done in Section.5, where the motor-tachometer shaft stiffness was estimated from the frequency response plots. Apart from parameter identification, the new tachometer model has significant implications in terms of controller design for achieving close-loop stability. These issues are discussed in the following section.

## 7. CONTROL SYSTEM DESIGN

### 7.1 Introduction

The objective of this exercise in control system design is to achieve a closed loop stable servo system for positioning the load inertia accurately using tachometer feedback, with reference to the system described in Section 6 (Figure 6.1). We know that compliance in a system, if not accounted for adequately in the controller design, leads to closed loop instability [4, 6, 9, 10], which in this case manifests itself as a high-pitch ringing.

We want to make sure that the compensator addresses all the high frequency open-loop poles and zeros resulting from flexible elements and that the compensated close-loop system has no poles on the right side of  $s$ -plane. It is observed that, if there is a high frequency pole in the open-loop system, its effect can never be completely eliminated. Since close-loop poles lie on the root-loci emanating from open-loop poles, there will be corresponding high frequency poles in the close-loop system as well. This is further clarified in the following sections. Nevertheless, by means of appropriate compensator design, we usually can ensure that the effect of these closed-loop poles on system stability is not detrimental. For close-loop stability, the closed-loop poles should all lie on the left side of the  $s$ -plane. If, for any reason, the closed-loop poles get too close to the imaginary axis or, even worse, spill over into the right side of the  $s$ -plane, then we can expect the undesirable phenomenon of high-frequency ringing in the closed-loop operation of the system. Since the objective is to eliminate this high frequency ringing during high-speed and high-precision closed loop operation, we shall proceed with the above discussion in mind.

The following three issues make the control design for the system in consideration interesting as well as complex:

- 1) This is a case of multiple inertias connected by flexible elements, with the sensor and actuator being noncolocated. While the torque is applied to the motor rotor, the angular measurement is made at the tachometer rotor. This necessitates the study of colocated and non-colocated systems.

- 2) The tachometer does not precisely measure the tachometer-rotor angular velocity. The tachometer has sensor dynamics, which adulterates the velocity signal and reshuffles the system zeros (as discussed earlier in Section 5). In fact the tachometer dynamics makes the system a non-minimum phase system, since some zeros introduced by the tachometer lie on the right hand side of the  $s$  plane.
- 3) Although while measuring the tachometer rotor angle, we are trying to position the load inertia. Normally, it is possible to control only those system states that can be measured or estimated. In this case we are trying to control the load position, which is not actually being measured. In this context, it is important to note that, since the system is relatively very stiff, positioning the motor/tachometer rotor will lead to a positioning of load inertia. If tachometer angle is used for feedback control, then the tachometer rotor will attain the commanded position very quickly, while the load inertia may have a slightly higher settling time. If ensuring closed-loop stability is the primary objective (i.e. eliminate high-pitch ringing) then this is not a problem. As long as any one transfer function (say tachometer angle vs. motor input torque) is used for designing a stable closed loop, the entire system is stabilized. All poles of all the close-loop transfer functions will have poles restricted to the left side of the  $s$ -plane. Despite this, if very fast and accurate positioning of the load inertia were the main concern, then it is a better choice to measurements at the load end rather than the motor end. Once again if we design a suitable controller to make the load-angle vs. motor-torque transfer function stable in close-loop, the entire system becomes stable i.e., there are no unstable poles in any transfer function of the system, and hence no high frequency ringing. But now motor and tachometer inertias shall have a longer settling time.

Before we deal with the actual system, let us investigate the above three issues one by one for ease of comprehension. Once we understand each one of these individually, we shall be able to study the combined effect of all these on the system in consideration.

## 7.2 Colocated and Noncolocated Control

### 7.2.1 Two-mass single-spring system

Although there will be damping (material, viscous or Coulomb) present in any real system, for the following discussion the damping terms have been neglected. Since the present objective is to study the occurrence and significance of poles and zeros in a system, this assumption is acceptable.

Throughout the following discussion, the term ‘pole’ should be interpreted as a complex-conjugate pole pair and ‘zero’ should be interpreted as a complex-conjugate zero pair.

For simplicity, initially the following two-mass single-spring system is considered. Free body diagrams for each mass are drawn.

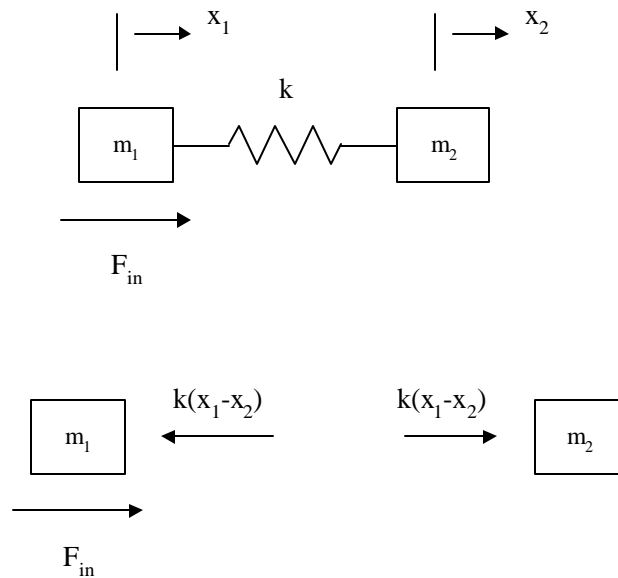


**Figure 7.1** Two-mass single-spring system

Application of Newton's II Law leads to,

$$\begin{aligned} F_{in} + k(x_2 - x_1) &= m_1 \ddot{x}_1 \\ k(x_1 - x_2) &= m_2 \ddot{x}_2 \end{aligned} \tag{7.1}$$

After a few algebraic manipulations, we obtain the following transfer functions

$$\frac{x_1}{F_{in}} = \frac{m_2 s^2 + k}{s^2 [m_1 m_2 s^2 + k(m_1 + m_2)]} \quad (7.2)$$

$$\frac{x_2}{F_{in}} = \frac{k}{s^2 [m_1 m_2 s^2 + k(m_1 + m_2)]}$$

$$\frac{x_2}{x_1} = \frac{k}{m_2 s^2 + k} \quad (7.3)$$

Thus, the pole frequency is  $\sqrt{\frac{k}{m_2} \left(1 + \frac{m_2}{m_1}\right)}$ , and the zero frequency is  $\sqrt{\frac{k}{m_2}}$  (7.4)

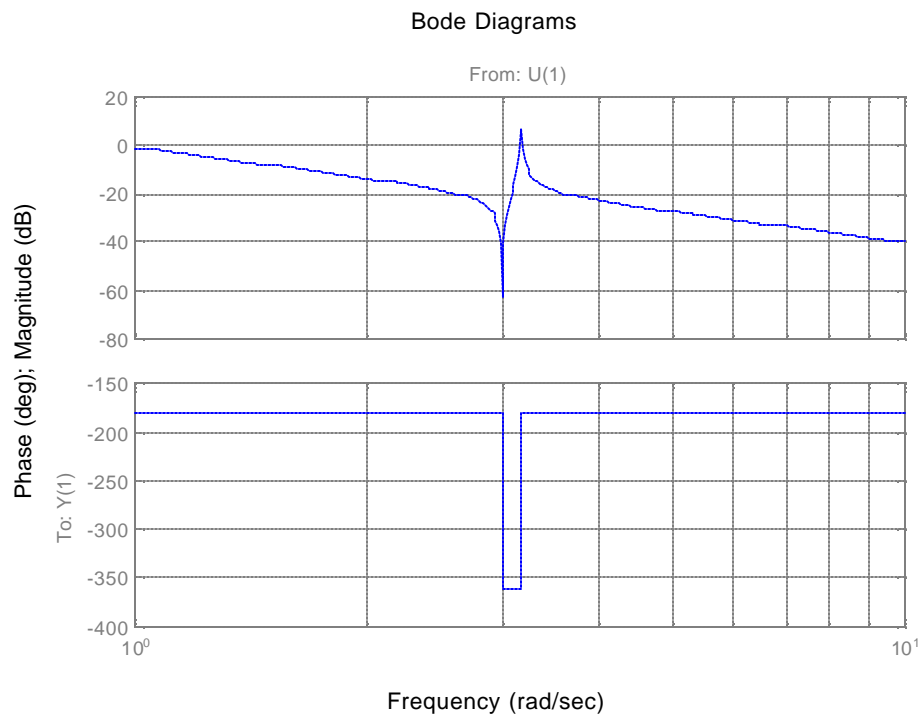


**Fig 7.2 Bode plot for  $x_1 / F_{in}$  transfer function**

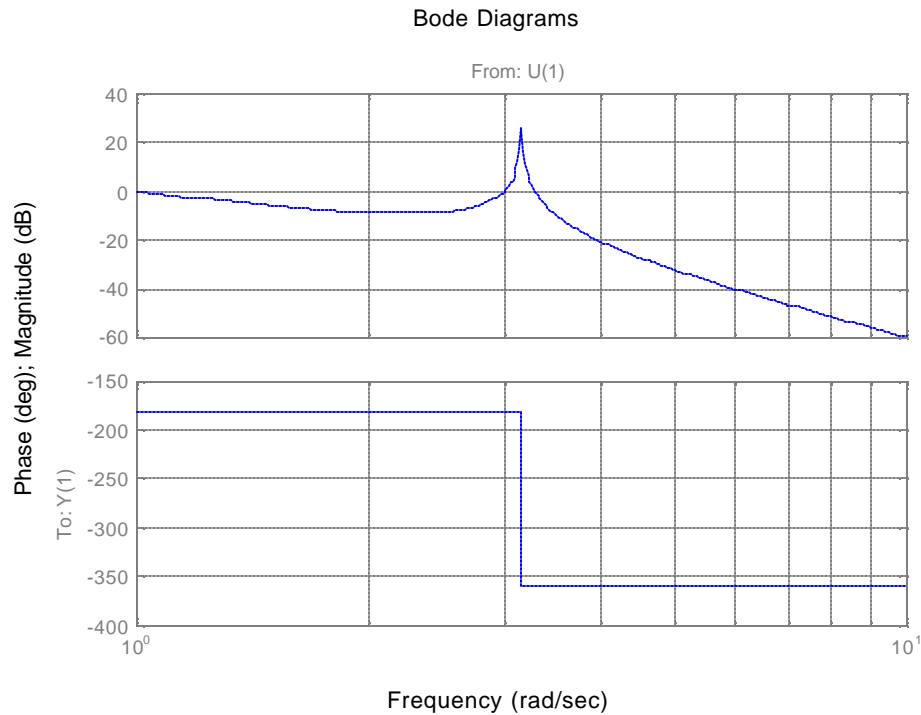


**Fig 7.3 Bode plot for  $x_2 / F_{in}$  transfer function**

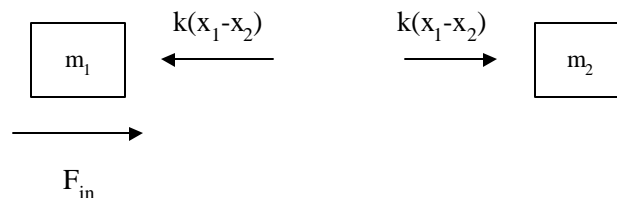
In this two-mass single-spring case, the  $x_1 / F_{in}$  transfer function is referred to as a collocated transfer function, since the actuator and sensor are mounted on the same mass. Whereas the  $x_2 / F_{in}$  transfer function is referred to as the noncollocated transfer function since the sensor and the actuator are mounted on different masses. It is important to note that for the collocated case, each pole is preceded by a zero, and hence there are alternating poles and zeros along the imaginary axis in the root-locus diagram. Quite unlike this, for the noncollocated case, every pole is not preceded by a zero. Since, poles are characteristic of the system, each transfer function in the system (collocated as well as non-collocated) exhibits the same poles. On the other hand, zeros depend upon the sensor and actuator location. If the two are collocated then, as mentioned earlier, there are as

many zeros as the number of poles. If the two are not colocated then the number of zeros falls short of the number of poles of the system.

### 7.2.2 Open-loop characteristics: Physical significance of poles and zeros

Let us try to understand the physical significance of poles and zeros and subsequently relate this understanding to the mathematically obtained conclusions. Based on the discussions in Section 7.2.1, we make the following observations

1. For the two-mass system described earlier, while both the masses experience the pole, only mass-1 experiences a zero. Mass-2 doesn't see this zero. This is an interesting phenomenon. If we look at the Free Body Diagrams of the two masses



we notice that, for mass-1 there can arise a situation, when the phases and magnitudes of the excitation force and the spring force are such that they exactly cancel out, i.e.

$$F_{in} = k(x_1 - x_2)$$

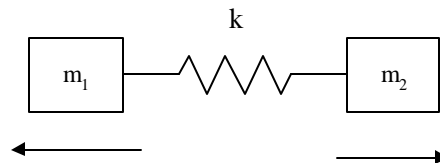
In such a situation (the reason why such a situation HAS to arise shall be discussed in the next point), mass-1 experiences a zero. Since mass-2 does not see the excitation force directly, it can never witness a complete force cancellation and hence never sees a zero. All that this argument says is, if at all a zero occurs, it shall be experienced only by mass-1 and not by mass-2. The following point explains why a zero HAS to occur.

2. A pole in a mechanical system represents a frequency at which some flexible element in the system is in a state of resonance. Hence the number of poles in the

system transfer function is equal to the number resonance modes of the system. Poles are characteristics of the system and are therefore experienced by all the masses. Once again referring to the two-mass single-spring system which has only one pole corresponding to a resonance in the spring. Let us first try to understand what this resonance physically means. At the resonance frequency, an infinitesimally small excitation force produces a large sustained motion in the system. Ideally, if there is no energy loss, then the system should exhibit violent oscillations even for zero excitation force. If the excitation force, which is also the net external force on the system, is zero, then total momentum of the system has to be conserved, i.e.,

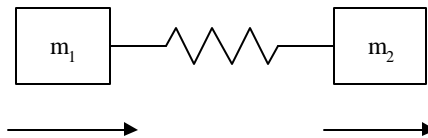
$$m_1 \dot{x}_1 + m_2 \dot{x}_2 = 0 \quad \Rightarrow \quad m_1 \dot{x}_1 = -m_2 \dot{x}_2$$

during resonance. This shows that at the resonance frequency, the two masses move  $180^\circ$  out of phase.



Now let us take a look at what happens at lower frequencies, and visualize the state of the system while gradually increasing the frequency.

*Stage I: Rigid Body; excitation frequency close to 0*



At low frequencies the two bodies move in phase with each other as though they were rigidly fixed. This is called the rigid body mode ( $\dot{x}_1 = \dot{x}_2$ ). Referring to equations **Error! Reference source not found.**, we conclude the following

$$\begin{aligned}\ddot{x}_1 &= \ddot{x}_2 = \ddot{x} \\ F_{in} &= (m_1 + m_2)\ddot{x}\end{aligned}\tag{7.5}$$

*Stage II: Resonance; excitation frequency close to pole frequency*

Between the initial stage (Stage I) when the two masses move in phase, and the resonance stage (Stage II) when the masses move out of phase, there has to be an intermediate stage where a transition from synchronism to asynchronism occurs. One of the two masses that are moving in phase has to come to a complete stop and then start moving in the opposite phase. This stage corresponds to a zero occurs at the zero frequency. As explained in the previous section, if there is a zero stage, the zero shall be experienced by mass-1 and not mass-2.

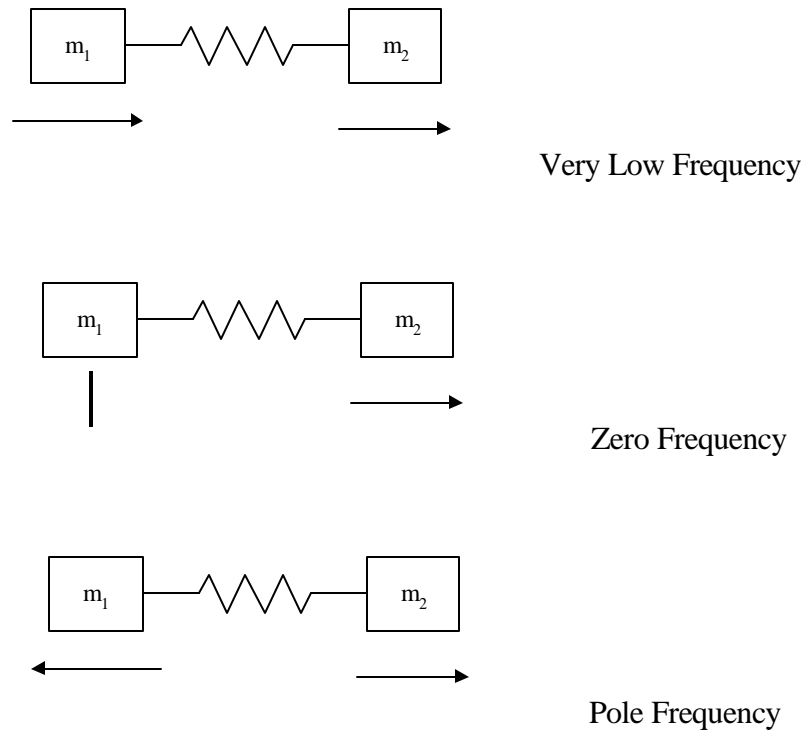


**Figure 7.4 System frequency response when excitation force is applied on mass-1**

This observation is verified by the transfer function between  $x_2$  and  $x_1$ ,

$$\frac{x_2}{x_1} = \frac{k}{m_2 s^2 + k}$$

and it becomes very clear from the Bode Plot presented in the following figure

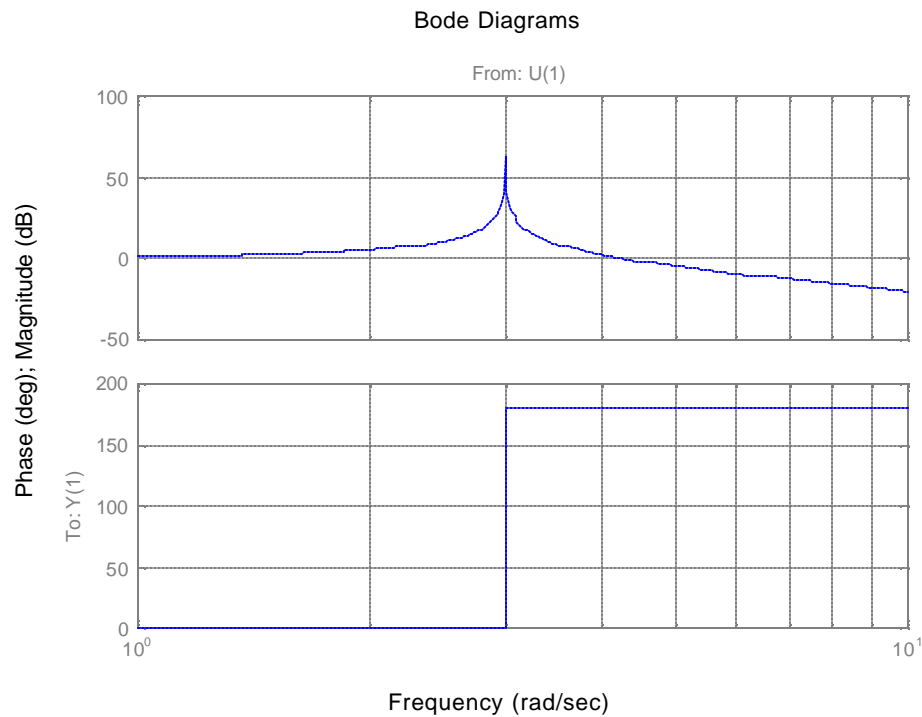


**Figure 7.5 Bode plot for  $x_2 / x_1$  transfer function**

Thus, zero frequency is the frequency at which the masses lose synchronism and fall out of phase. This leads to a very significant conclusion: For a purely mechanical system, a resonance frequency is always preceded by a zero frequency. For a resonance to occur, the two masses have to be out of phase, and this happens only at the zero frequency. Hence, since the zero sets the stage for the resonance, it has to occur before the pole. In other words, the zero frequency is always less than the pole frequency. What we have concluded by physical reasoning is exactly the same as what was predicted by

mathematical derivation in expressions (7.2)-(7.4). A similar discussion on poles and zeros is provided by Welch [4].

### 7.2.3 Closed-loop characteristics: Stability Analysis

In the previous sub-section, we discussed the open-loop characteristics of the two-mass single-spring system. In this section we shall try to concentrate on the closed-loop characteristics of the same system. We shall investigate the stability of the closed loop system by looking at the root-locus and frequency plots of the open loop system. Once again, let us rewrite the two relevant transfer functions for the system

$$\frac{x_1}{F_{in}} = k_1 \frac{s^2 + z_1^2}{s^2(s^2 + p_1^2)} \quad \text{Colocated Case}$$

$$\frac{x_2}{F_{in}} = \frac{k_2}{s^2(s^2 + p_1^2)} \quad \text{Noncolocated Case}$$

$$z_1 < p_1 \quad \text{(shown earlier)}$$

$$\frac{x}{F_{in}} = \frac{1}{s^2} \quad \text{Rigid Body Case}$$

where  $z_1$  is the zero and  $p_1$  is the pole, as given by expressions (7.2)-(7.4).

Each of these cases is studied individually and the compensator designs that make the respective systems stable in close-loop are presented. We also consider the case of a rigid body that has no flexible elements and compare it with the above two cases in terms of closed loop stability.

$$\text{Rigid Body Case:} \quad \frac{x}{F_{in}} = \frac{1}{s^2}$$

Without any compensator the root-locus and frequency plots for the system are as follows,

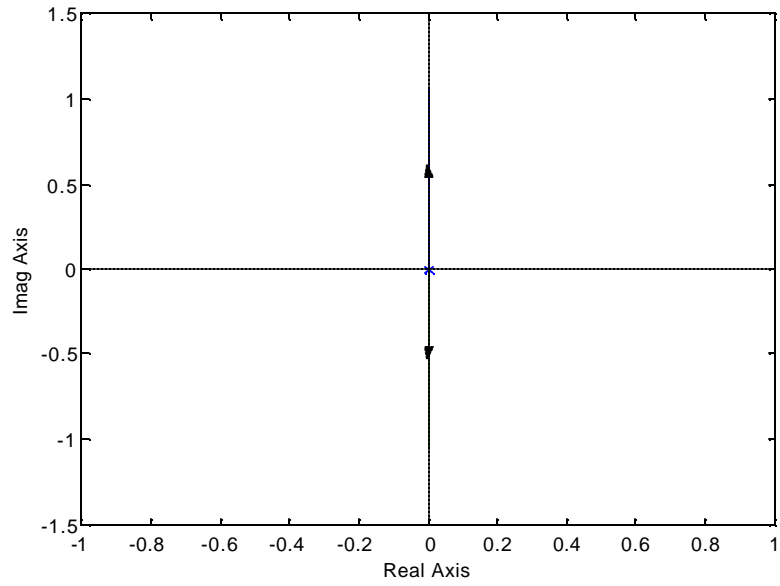


**Fig. 7.6(a) Root-locus for the rigid body case ( $\frac{1}{s^2}$ )**

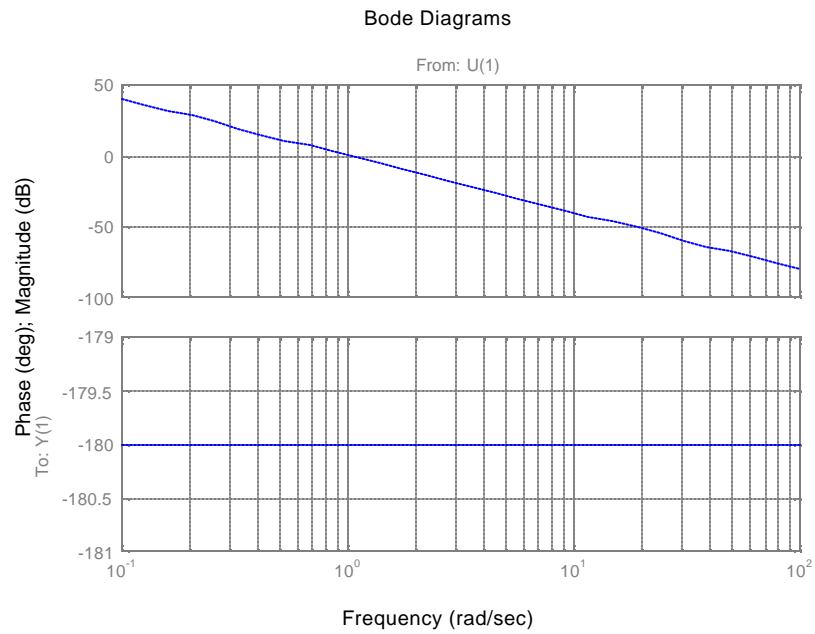


**Fig. 7.6(b) Bode plots for the rigid body case ( $\frac{1}{s^2}$ )**

From the root locus it is clear that the system is marginally stable for any value of gain, since the close-loop poles always lie on the imaginary axis. This is confirmed from the Bode plots, which indicate that for any gain, the Phase Margin is always zero. Hence the system is at the margin of stability. If we add a lead compensation to the plant, then the above two plots get modified as follows:

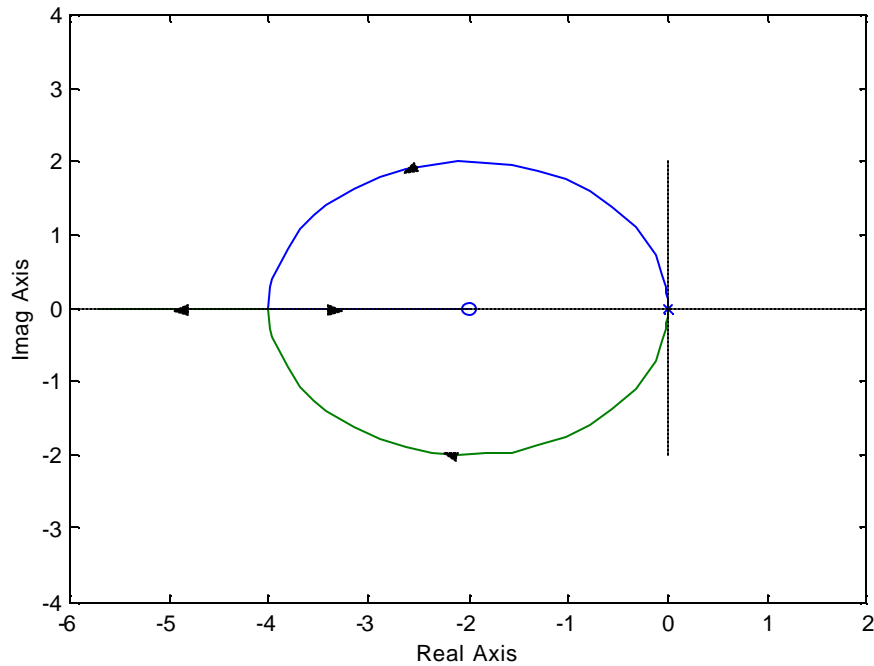


**Fig. 7.7(a) Root-locus for the rigid body case with lead compensation  $\left(\frac{s+2}{s^2}\right)$**

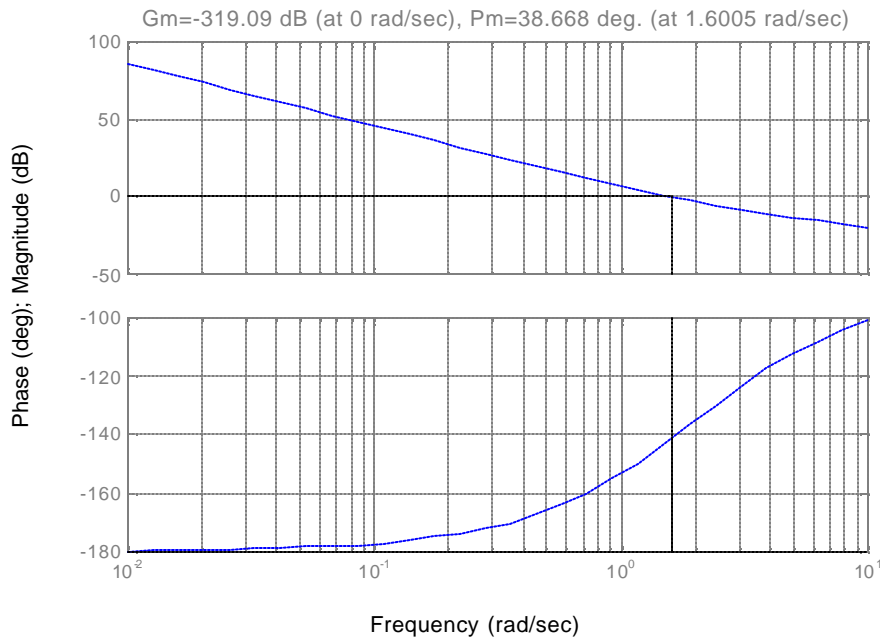


**Fig. 7.7(b) Bode plot for the rigid body case with lead compensation ( $\frac{s+2}{s^2}$ )**

From these new plots it is clear that the lead compensator (real zero in the numerator) stabilizes the closed loop system by adding phase to the open-loop system. In the root-locus plots, the compensator zero has pulled the root-loci branches to the left side of the  $s$ -plane, thus making the closed loop system stable for any gain. On the other hand looking at the Bode plot we see that the system has infinite Gain Margin, since the phase asymptotically approaches  $-180^\circ$ . Also for any gain and therefore for any cross-over frequency, there is a positive Phase Margin. When the gain is very low, the cross-over frequency is also low which leads to a very small Phase Margin. This corresponds to the fact that now the closed-loop poles on the root-locus plot are very close to the imaginary axis. For high gains, the Bode plots predict a maximum phase margin of  $90^\circ$ . On the root-locus this corresponds to the fact that now the close-loop poles lie on the negative real axis, thus making the system very stable. In any case, we notice that it is very easy to stabilize the rigid body mode transfer function. Thus if there are no flexible elements in a

system, then close-loop instabilities are easily avoided. Now let us see how the presence of a spring in the system changes this situation.

*Colocated Case:* 
$$\frac{x_1}{F_{in}} = \frac{s^2 + z_1^2}{s^2(s^2 + p_1^2)}$$

For the colocated case we observe that other than the two poles at the origin, the system also has a pole-zero pair. As was observed earlier, the zero frequency is always less than the pole frequency. In the case of multiple flexible elements, an important feature of the colocated transfer function is the pole-zero alternation as one moves along the imaginary axis. This property will be of immense use in the design of a compensator as shall be seen shortly.

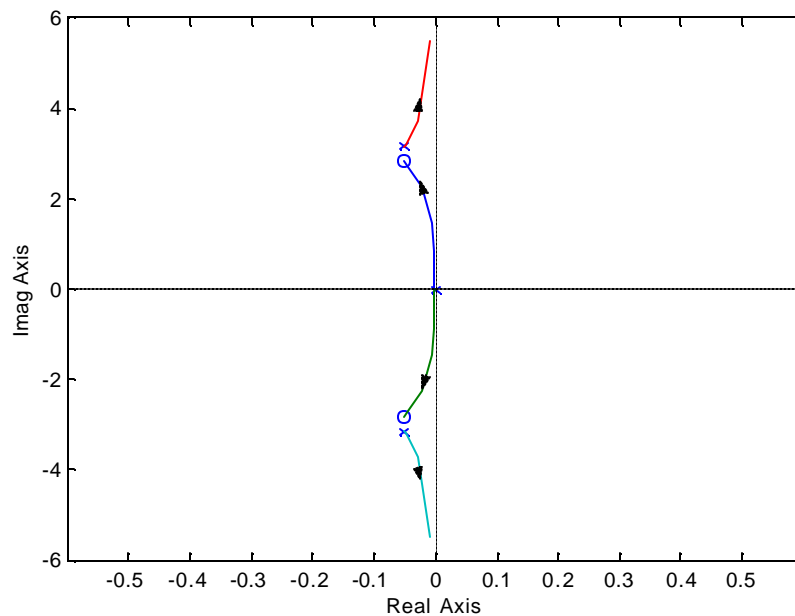


**Fig. 7.8(a)** Root-locus plot for the uncompensated colocated system  $\left(\frac{s^2 + z_1^2}{s^2(s^2 + p_1^2)}\right)$

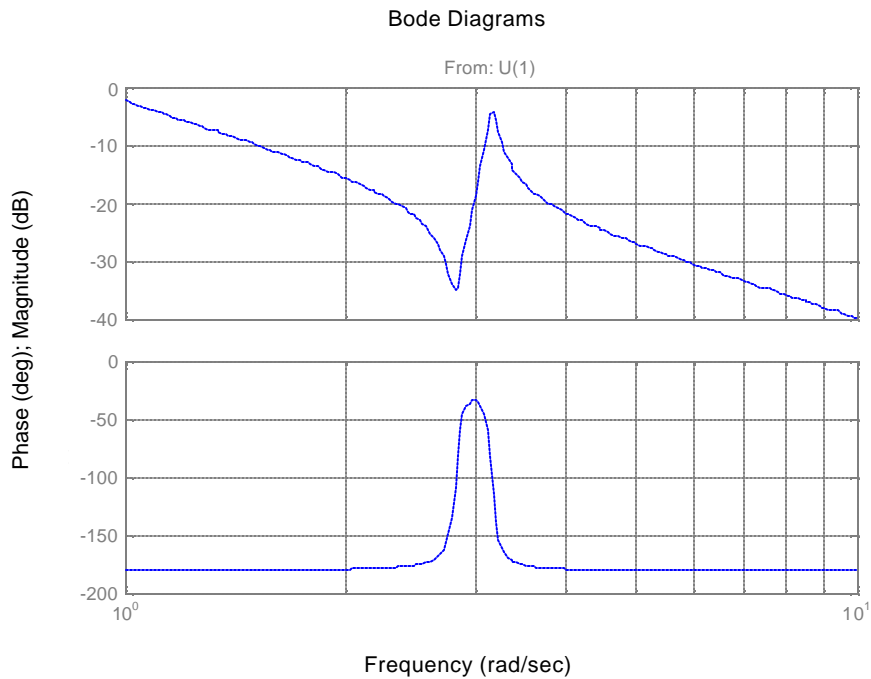


**Fig 7.8(b) Bode plots for the uncompensated collocated system**  $\left( \frac{s^2 + z_1^2}{s^2 (s^2 + p_1^2)} \right)$

Note that a small amount of damping has been added (although not indicated in the transfer function) while obtaining these plots to make them more realistic. From the root-locus of the uncompensated collocated system, it is evident that the system will only be marginally stable for any value of gain. Similarly, the Bode plots show that for any open-loop gain the Phase Margin will be very small, nevertheless positive. Next, we study the effect of a lead compensator on this system.

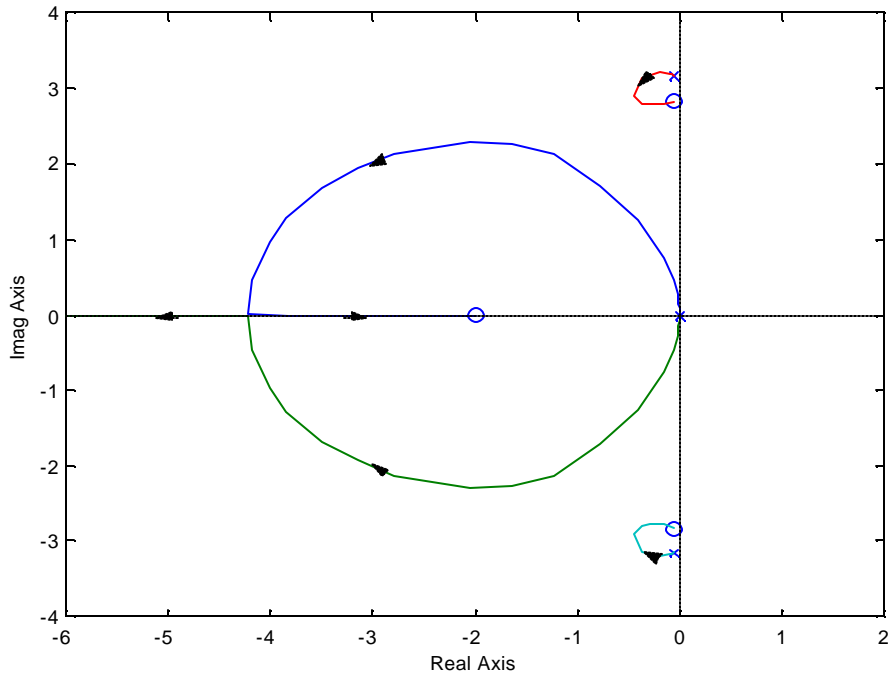


**Fig 7.9(a) Root-locus plot for the compensated collocated system:**  $(s+2) \frac{s^2 + z_1^2}{s^2(s^2 + p_1^2)}$

Here the root-locus indicates that the system will be unconditionally stable for all gains. For very low and very high gains, the closed-loop poles are quite close to the imaginary axis. These observations are confirmed from the Bode plots as well. For any value of gain the system has a positive gain margin. For a low open-loop gain, resulting in a low crossover frequency, the phase margin (although positive) is very close to zero. Once again, for the collocated case we see that it is fairly easy to stabilize the closed loop system by means of a simple lead controller. It is important to mention here that this has been possible only due to the fact that the zero occurs before the pole, which adds phase to the system at the right frequency. Had this not been the case, close-loop instability would have existed.

### Bode Diagrams

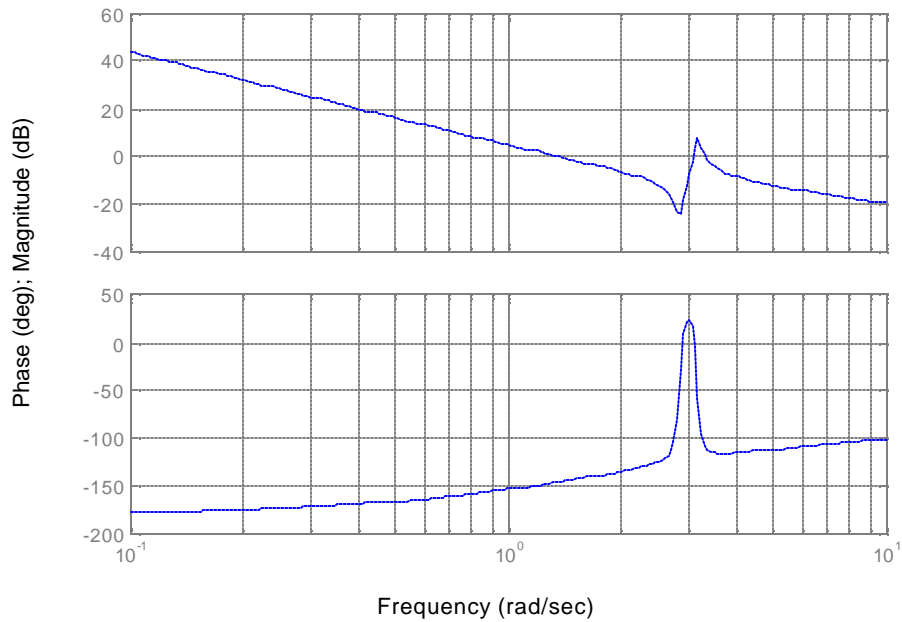


**Fig. 7.9(b) Root-locus plot for the compensated collocated system:**  $(s+2)\frac{s^2+z_1^2}{s^2(s^2+p_1^2)}$

*Noncolocated Case:* 
$$\frac{x_2}{F_{in}} = \frac{1}{s^2(s^2+p_1^2)}$$

In the noncolocated case, a distinct feature is that not all poles have a zero that precedes them. In fact for the two-mass single-spring case, the noncolocated transfer function has no zeros at all. The root-locus and bode plots for this case are presented in the following figures. Clearly, from the root-locus the uncompensated system is unstable for any gain, high or small. At the same time, Bode plots indicate that for any open-loop gain, the Phase margin will be negative. For extremely small gains, the phase margin approaches zero but from the negative side. Hence the system is always unstable.

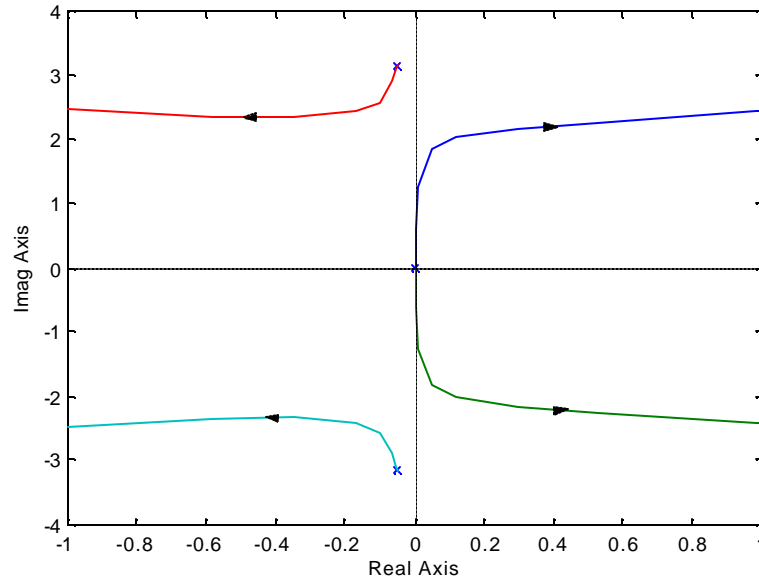


**Fig. 7.10(a) Root-locus for the uncompensated noncolocated system  $\left(\frac{1}{s^2(s^2 + p_1^2)}\right)$**

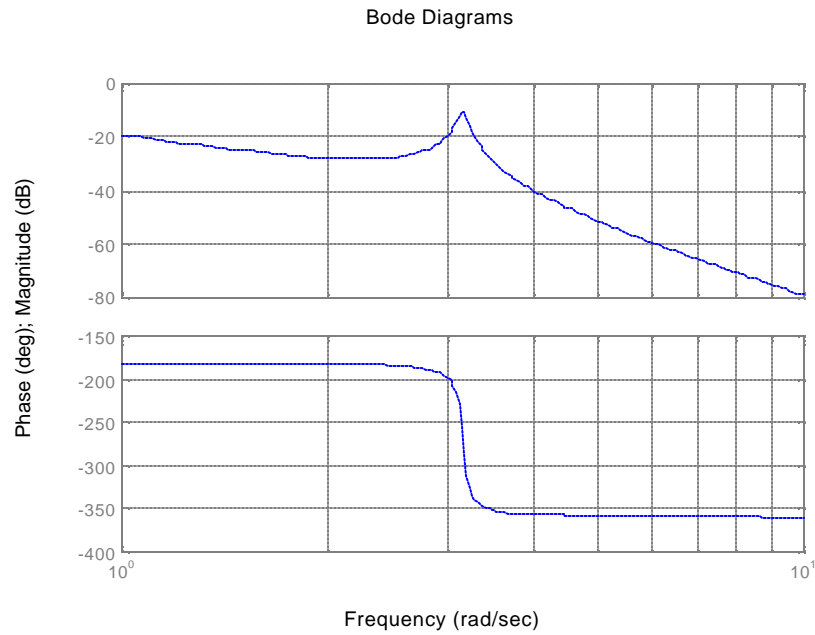


**Fig. 7.10(b) Bode plots for the uncompensated noncolocated system  $\left(\frac{1}{s^2(s^2 + p_1^2)}\right)$**

As a next step, let us see what happens to the stability of this noncolocated system in the presence of the same lead compensator that worked well for the previous two cases of rigid body system and collocated system.

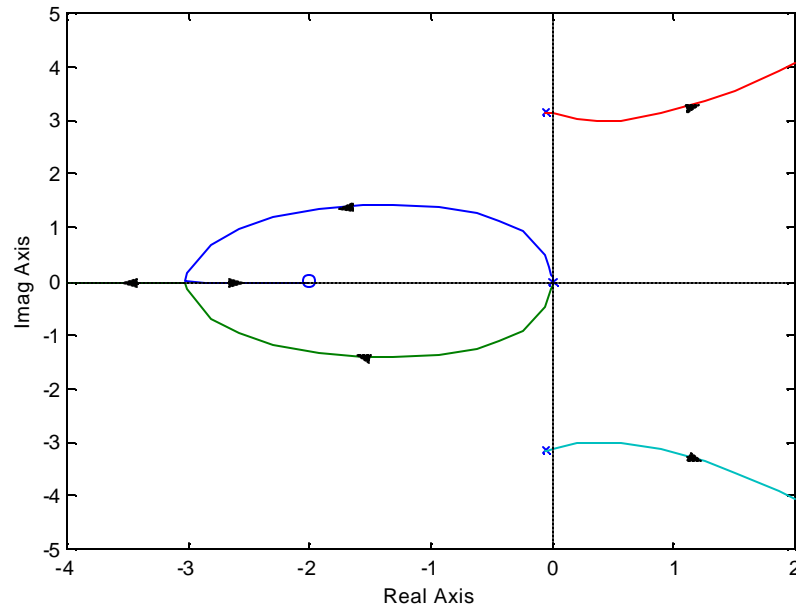


**Fig. 7.11(a) Root-locus plot for the lead compensated noncolocated system**

$$\left( (s+2) \frac{1}{s^2(s^2 + p_1^2)} \right)$$

The root-locus reveals that the lead compensation is of little use in ensuring close-loop stability. Except for very small gains (that too only when damping is present in the system), a couple of close-loop poles always lie in the right hand side of the s-plane. Looking at the corresponding Bode plots, we can make similar conclusions about the close-loop stability. The gain margin is completely dependent upon damping of the poles. If there were no damping at all, then the gain margin would be less than unity for any value of open-loop gain. In case damping is present, we can reduce the open-loop gain enough so that there is some gain margin. But this stability comes at the cost of system speed. Reducing the open-loop gain reduces the cross-over frequency which in turn limits the closed loop bandwidth. Thus makes the system response very slow. While this might

be too slow to meet the settling-time specification, a low cross-over frequency is unavoidable if we expect to keep the gain at the resonance frequency below unity.

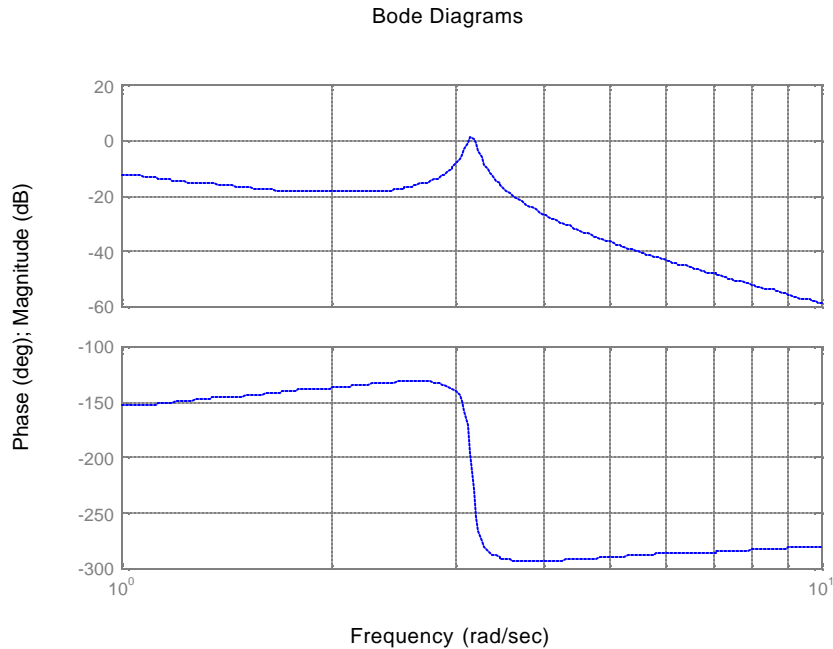


**Fig. 7.11(b) Bode plots for the lead compensated noncolocated system**

$$\left( (s+2) \frac{1}{s^2(s^2 + p_1^2)} \right)$$

So right away we realize that achieving closed loop stability for a noncolocated system is not at all as simple as it is for a rigid body system or a colocated system. We have to explore other compensators for stabilizing the system. Essentially we need to add more phase to the system. Learning from the colocated system transfer function, one option is to place external compensator zeros next to poles in the noncolocated system and make it behave like a colocated system. This is called a notch-filter compensator [4,10]. The compensator zero frequency has to be lower than the plant resonance frequency. Let us see the effect of a notch filter compensator on the stability of the system. The

compensator is now given by:  $(s+2) \frac{(s^2 + z^2)}{(s+25)^2}$

where  $z$  is compensator zero such that  $z < p_1$

The overall open-loop transfer function for the compensated system now becomes

$$(s+2) \frac{(s^2+z^2)}{(s+25)^2 s^2 (s^2+p_1^2)}$$

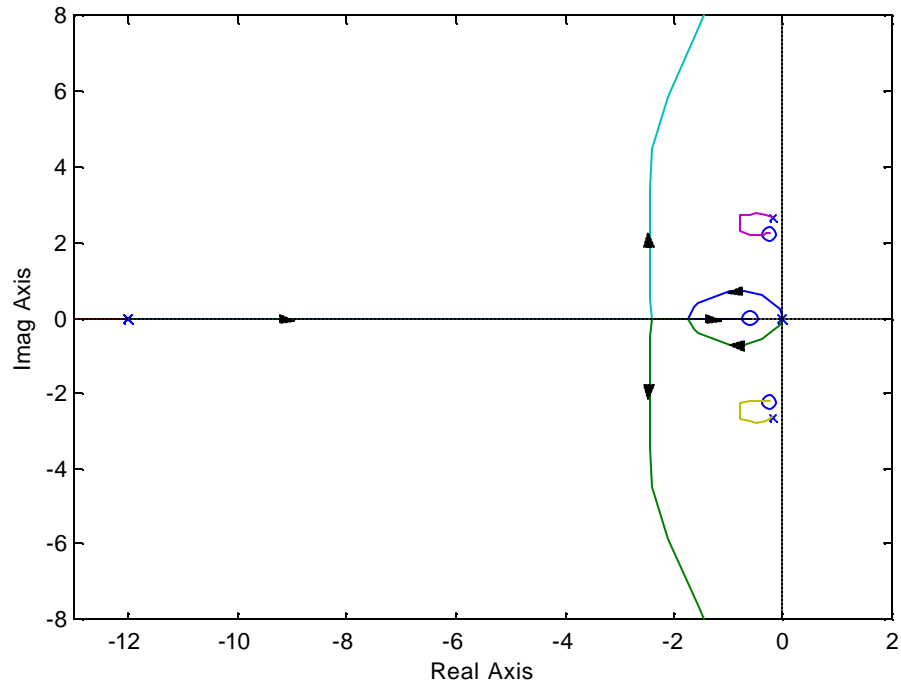


**Fig. 7.12(a) Root-locus plot for the notch compensated noncolocated system**

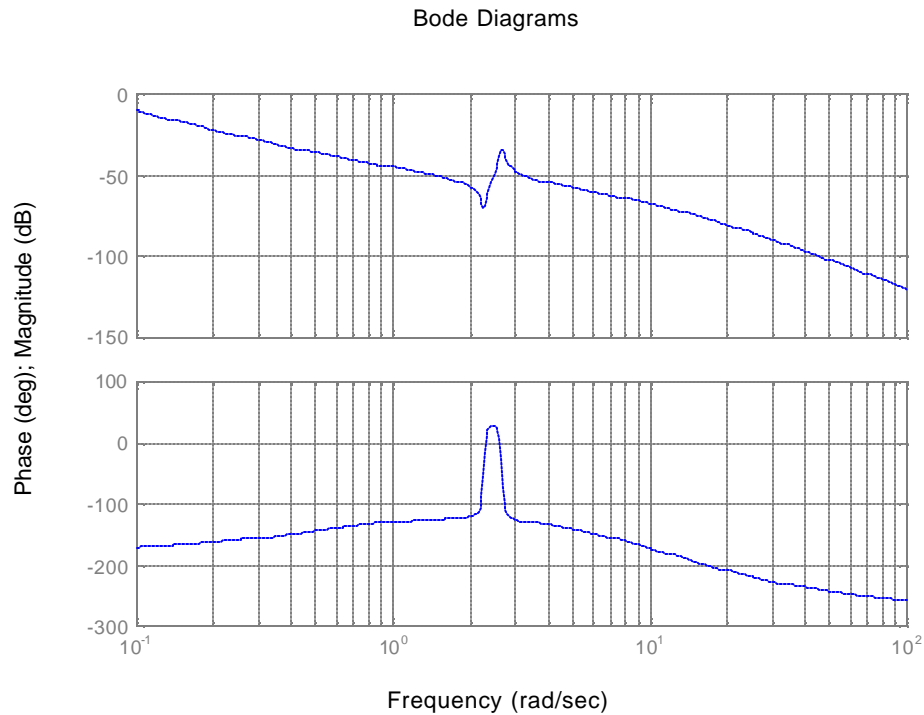


**Fig. 7.12(b) Bode plots for the notch compensated noncolocated system**

The two real poles in the compensator are necessary because the compensator zeros add gain to the system at high frequencies thus making it susceptible to noise. The two poles are placed far enough on the real axis so that their effect on stability is minimal, but at the same time they ensure noise rejection at high frequencies. The zeros essentially add a 180 degrees phase at frequencies close to the system resonance frequency thus making it close-loop stable. The problem with the resonance pole is that it leads to a phase lag of 180 degrees, which becomes detrimental for the close-loop stability.

From the above root-locus plots we conclude that the system is now stable except for extremely high gains. The bode-plots indicate a positive phase margin for most values of open-loop gain. For very high gains though, the phase margin becomes negative. The notch-filter compensator for noncolocated systems is robust as long as the compensator zero frequency is less than the plant resonance frequency. In case some parameter variation causes the compensator zero to fall after the pole, a phenomenon called zero-pole flipping, the system stability is jeopardized. Such an effect is extremely detrimental

for the system as is shown in the following figures. Pole-zero flipping may also occur with the natural zeros in a non-colocated system. This issue is discussed in the following sections.

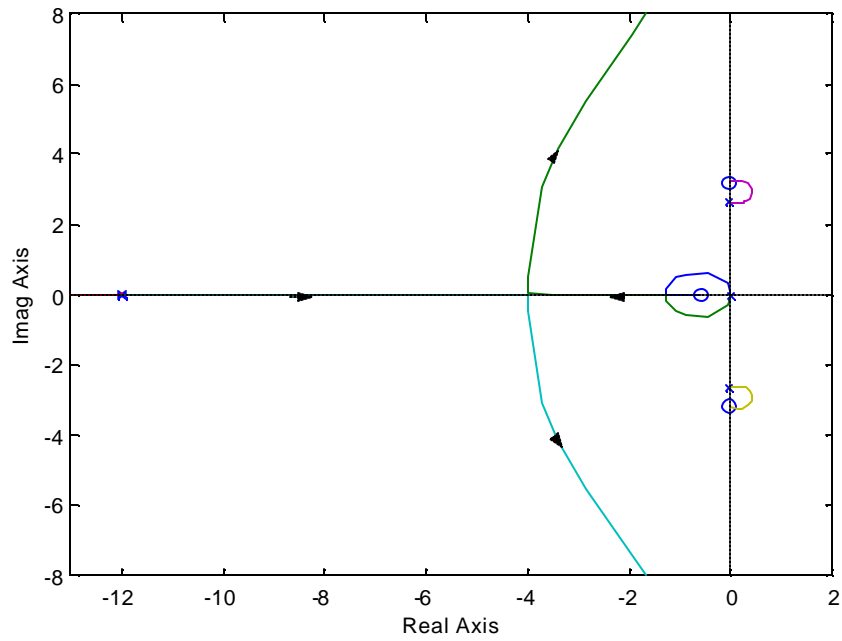


**Fig. 7.13(a) Root-locus for the notch compensated noncolocated system in the presence of pole-zero flipping**

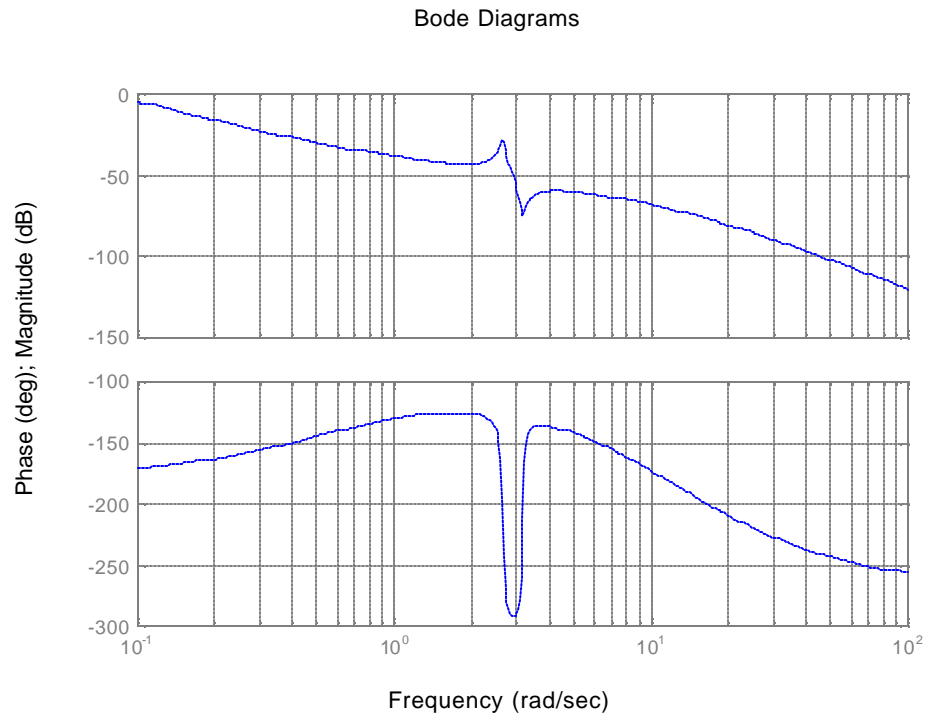


**Fig. 7.13(b) Bode plots for the notch compensated noncolocated system in the presence of pole-zero flipping**

As is clear from the above plots, the compensator zero does add phase to the system, but at such a frequency that the phase margins are not improved at all. In fact, when a pole-zero flipping occurs, the system becomes unconditionally unstable. In case the system has some damping, the closed-loop system may be stable for very low or very high gains. This is evident from the Bode plots which show that a positive phase margin exists for very low and high gains.

In such a situation the compensator is no longer robust. Hence care should be taken while implementing a notch-filter controller. In fact, for a robust compensator design, many authors recommend the use of an optimal state-space controller [6,10]. A robust Linear Quadratic Gaussian (LQG) compensator design is presented by Cannon [10].

## 7.2.4 Multiple Mass Systems

We now extend the ideas developed in Sections 7.2.1-7.2.3 to multiple mass systems. For a multiple-mass system with multiple flexible elements, like the one shown in Fig. 7.14

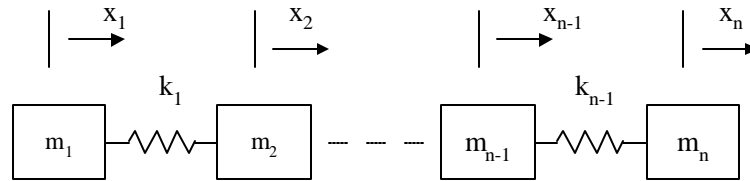


**Fig. 7.14 Multiple-mass multiple-spring system**

the system has as many resonance modes as the number of flexible elements (as long as there are no closed chains in the system). Each of these resonance modes corresponds to a complex-conjugate pole pair.

From another perspective, the system has as many modes of motion as the degrees of freedom of the system. Thus if the system has four masses then there will be four complex-conjugate pole pairs (including the pair at origin which corresponds to the rigid body mode). Excluding the rigid body mode, the system therefore has three resonance modes. These resonance modes are characteristics of the system and hence are experienced by each mass in the system.

If an excitation force is applied on one of the masses in the above system, then we can obtain transfer functions between the various system coordinates  $(x_1, x_2, \dots, x_n)$  and the input force. One of these will be a colocated case, wherein the actuator and sensor are mounted on the same mass. All other transfer functions are the noncolocated cases. Nevertheless, the poles of each of these transfer functions are the same, since poles are characteristic of the entire system. As was discussed in Section 7.2.1, to set the stage for each pole (i.e. resonance) a zero has to precede the resonance. Now this zero is

experienced only by some of the masses depending upon the actuator location, giving rise to colocated and noncolocated cases.

For the colocated case, the mass on which the actuator force is applied experiences all the zeros that precede the poles and hence the number of zeros in the colocated transfer function is equal to the number of non-zero poles of the system. It is important to note that for the colocated case, since each pole is preceded by a zero, there are alternating poles and zeros along the imaginary axis in the root-locus diagram. As seen earlier, this makes the control design problem very amenable. Even a simple lead compensator provides a robust control action.

On the other for the non-colocated cases, the number of zeros experienced by any mass falls short of the maximum possible number, by the number of coordinates (or masses) that separate the sensor and the actuator. Also in this case parameter variation can lead to the undesirable phenomena of pole-zero flipping. As an example consider the following four-mass system.

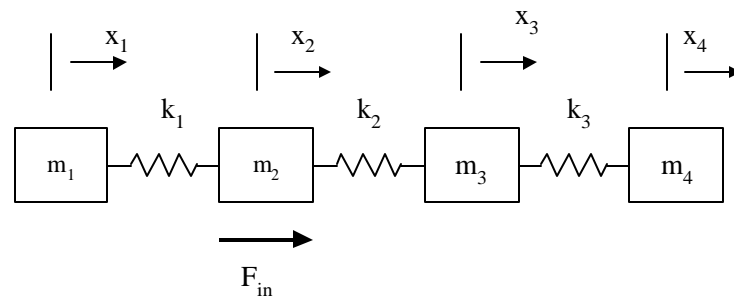


**Fig. 7.15 Four-mass three-spring system**

The system has three resonance modes and hence 3 non-zero complex-conjugate pole pairs. It also has one rigid body mode which results in a pole pair at the origin. While mass-2 experiences three zeros since the actuator force acts on it, the other masses experience fewer zeros. The  $x_1/F_{in}$  and  $x_2/F_{in}$  transfer functions have two zeros each, while the  $x_4/F_{in}$  transfer function has only one. The three resonance modes of the system can occur in any order depending upon the mass and spring stiffness values. The single zero in the  $x_4/F_{in}$  transfer function corresponds to a zero before one of the three resonance

modes. Since the order of the resonance modes can vary depending upon the system parameters, the single zero can occur before the first resonance, or between the first and second resonance, or between the second and third resonance. This phenomenon is known as pole-zero flipping and as was demonstrated earlier can jeopardize the close-loop system stability since it drastically changes the root-locus and frequency response plots. Therefore, during the compensator design for non-located systems it is necessary to be aware of this problem and make sure that the compensator is robust enough to handle this sudden change in phase and gain plots.

Let us see the close-loop behavior of this noncolocated transfer function in the presence of a lead compensator (which of course is not sufficient to stabilize the system). In the first case the zero lies between the first two resonance poles while in the second case it lies between the last two poles.

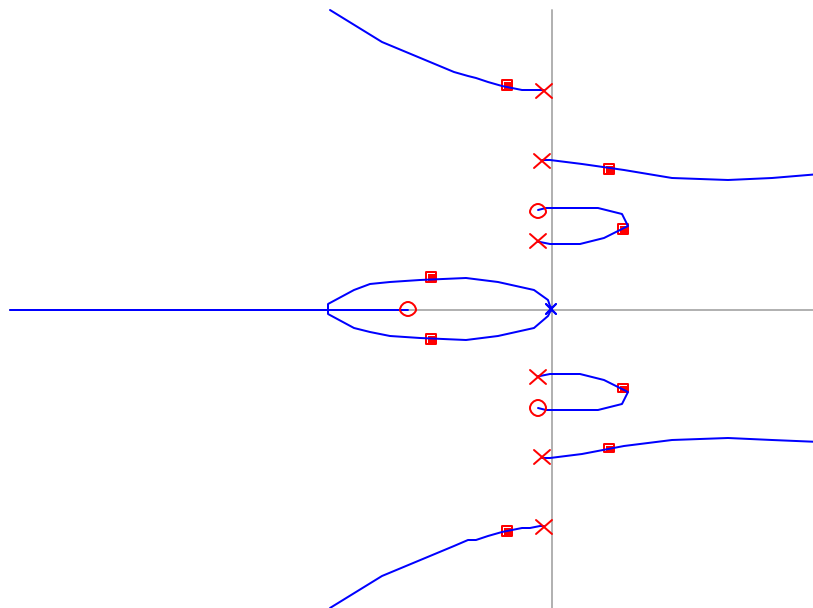


**Fig. 7.16(a) Pole-zero flipping in a noncolocated system**

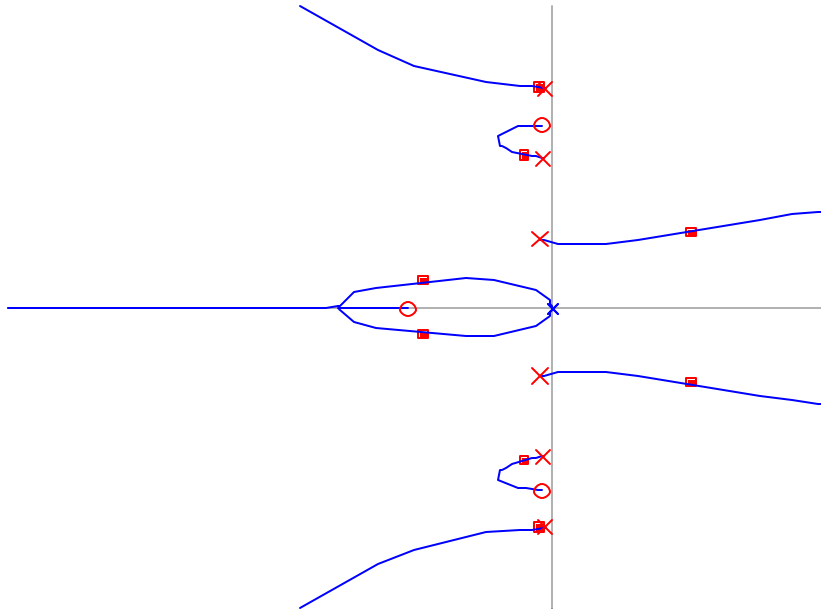


**Fig. 7.16(b) Pole-zero flipping in a noncolocated system**

### 7.3 Tachometer-Motor-Load System

Now that we have understood the fundamentals of colocated and noncolocated controls with reference to multiple-mass multiple-spring systems, we are in a position to focus our attention on the system in consideration, the tachometer-load-inertia system.

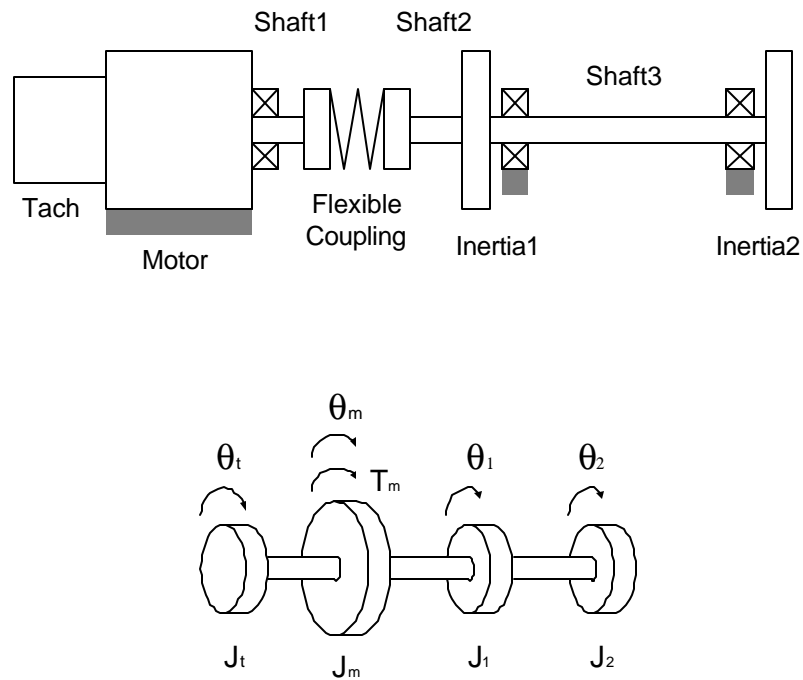


**Fig. 7.17 Physical System and Physical Model**

Since the actuator torque is applied at the motor rotor, and the speed is sensed at the tachometer, the transfer function is noncolocated. Referring to Section 6 and equations (6.1)-(6.2), we have the following transfer function for this system,

$$\frac{\mathbf{q}_t}{T_m} = \frac{[num]}{s^2 \cdot [den]} \quad (7.6)$$

where,

$$\begin{aligned}
[num] &= K [J_1 J_2 s^4 + (J_1 K_2 + J_2 K_1 + J_2 K_2) s^2 + K_1 K_2] \\
[den] &= s^6 [J_t J_m J_1 J_2] + \\
& s^4 [K_2 J_t J_m J_1 + K_1 J_t J_m J_2 + K_2 J_t J_m J_2 + \\
& \quad K J_m J_1 J_2 + K J_t J_1 J_2 + K_1 K_t J_1 J_2] + \\
& s^2 [K_1 K_2 J_t J_m + K K_2 J_1 J_m + K K_1 J_2 J_m \\
& \quad K K_2 J_2 J_m + K K_2 J_t J_1 + K K_1 J_t J_2 \\
& \quad K K_2 J_t J_2 + K_1 K_2 J_t J_1 + K K_1 J_1 J_2 + K_1 K_2 J_1 J_2] \\
& + [K K_1 K_2 (J_t + J_m + J_1 + J_2)]
\end{aligned} \tag{7.7}$$

Plugging in the parameter values listed in Table 6.1, we obtain the following poles and zeros for the system,

Poles	Zeros
0	
0	
-25 + 2615i	-25 + 2017i
-25 - 2615i	-25 - 2017i
-10 + 5406i	-10 + 5297i
-10 - 5406i	-10 - 5297i
-25 + 14019i	
-25 - 14019i	

The open-loop gain is 5.7. Since the system is noncolocated, only the first two resonance poles are preceded by zeros, the last one is not. If the tachometer had no dynamics then, expression (7.6) would represent the overall system transfer function and we would proceed to find a suitable controller that stabilizes the system in close-loop.

It should be mentioned here that in the modeling we have not accounted for any sort of damping for reasons stated earlier (Section 3). But at this stage we do introduce some

empirical values of damping at each of these poles and zeros to avoid singularities in the root-locus and bode plots. These damping values are estimated by matching the experimental frequency plots with the analytically predicted ones.

The actual root-locus for the open-loop system is as follows:

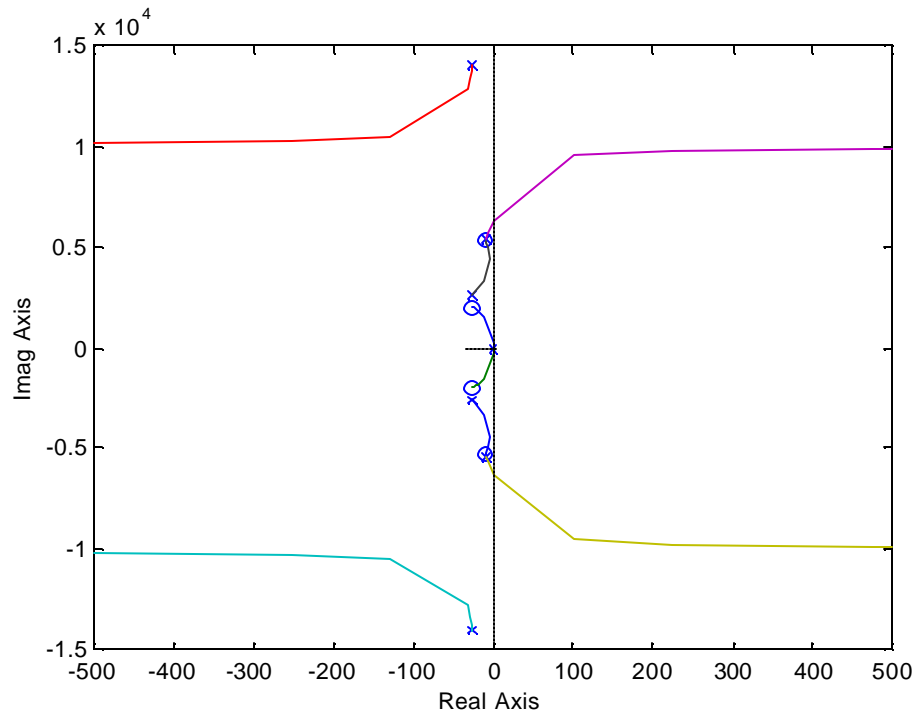


**Fig. 7.17(a)**  $\frac{q_t}{T_m}$  : Root-locus for the tachometer-motor-load mechanical system

For ease of visualization, the following exaggerated (yet qualitatively correct) plot (Fig 7.18(a)) of the same system. This provides a better picture of the pole and zero locations. Clearly the system is marginally stable in close-loop. In Fig. 7.18(b), we investigate how and to what extent can a lead controller help stabilize this system.

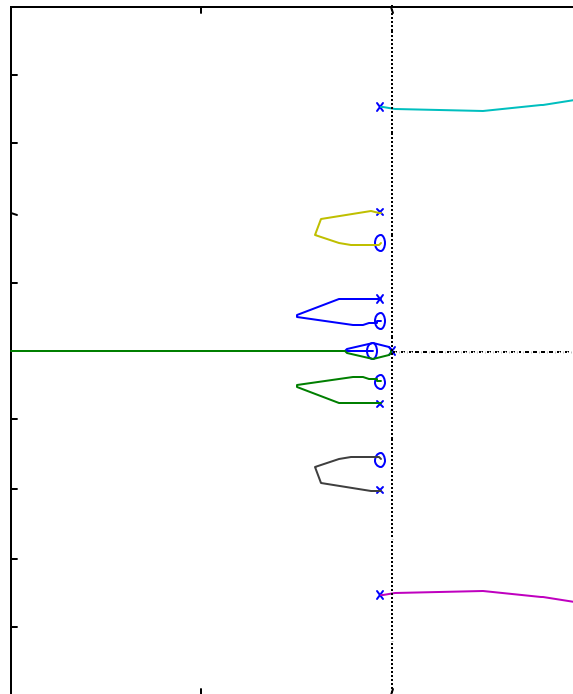
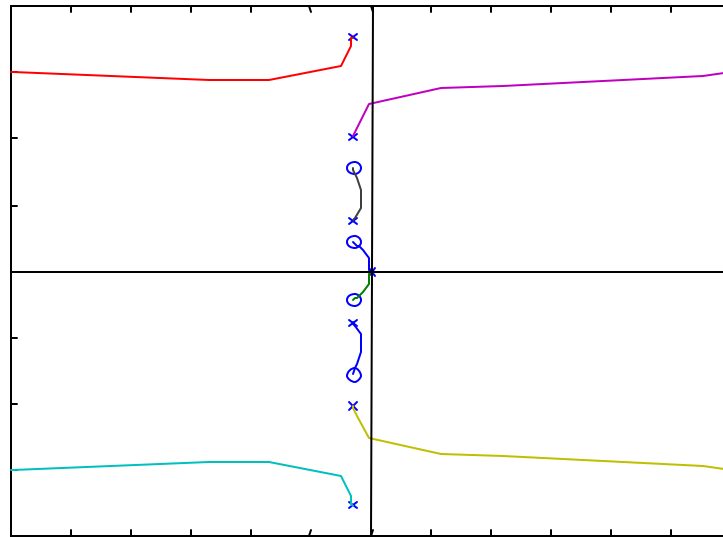


**Fig. 7.18 Root locus for (a) Uncompensated system (b) Lead compensated system**

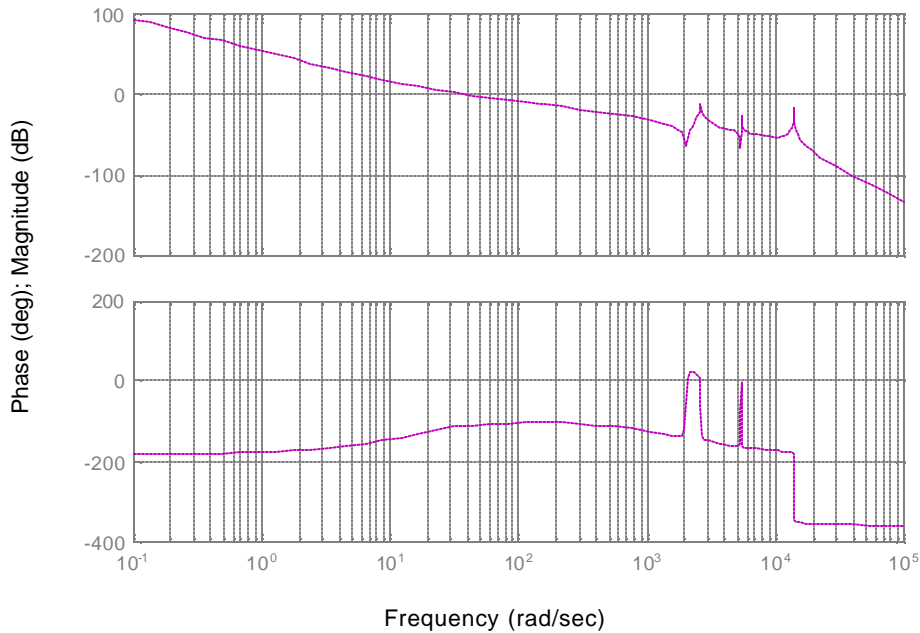


**Fig 7.19 Bode Plots for the system with lead compensation**

As expected, since the system is noncolocated, a lead compensator does not make sure that all the root-loci branches are on the left-hand side of the  $s$ -plane. Depending on the lead zero location, the root-locus can take various forms but there are two branches emanating from the last poles that always spill into the right-hand side. Nevertheless, it is interesting to note that since the pole and-zero frequencies are so high and because there is some damping present at the poles, we can get a reasonable closed-loop bandwidth without destabilizing the system. Since the poles lie so far out on the frequency scale, the open-loop gain can be increased still maintaining acceptable phase and gain margins. In the particular case illustrated in the bode plots above, a crossover frequency of 100 rad/sec is achieved using the following lead controller,

$$200 \frac{s+15}{s+1500}$$

This may or may not meet the desired rise time specifications. To achieve an even higher bandwidth without causing the system to go unstable, it may be advisable to use a notch

compensator or a state-space controller (as was discussed in Section 7.2.3). It is also noteworthy that the settling time is dependent on the first pole-zero pair location, since the corresponding close-loop pole will lie close to this pole-zero pair.

But, we have to step back and realize that the tachometer does not act as a pure gain; it adds sensor dynamics to the system. The fact that the tachometer reshuffles the original zeros of the system and adds further zeros to the overall transfer function changes the scenario completely. Referring back to Section 6, the overall transfer function with the tachometer dynamics included is given by

$$\frac{V_{tach}}{V_{in}} = \frac{K_{amp} [K_m s^2 (den) - K_r s (den) + K_t K_{tach} (num)]}{s (den)} \quad (7.8)$$

where (num) and (den) are the same as defined in expression(7.7)

Referring to Section 5 of this thesis, we know that the tachometer dynamics causes the system to have as many zeros as are the number of poles (including the pair at the origin). If there are four pairs of complex conjugate poles (and if  $K_m$  is positive, which it is for this particular set-up) then there will be 4 complex-conjugate zeros in the overall system transfer function. Since the system is no longer a purely mechanical but is now electromechanical in nature, the alternating sequence of poles and zeros on the imaginary axis is not assured. In fact we do observe the previously discussed phenomenon of pole-zero flipping in this case. Furthermore, some of these new zeros lie on the right-hand side of the s-plane making the system non-minimum phase and thus making the control system design much more difficult. Now the zeros no longer add phase to the system, they rather reduce phase from the system, which is a very unhealthy development.

Thus we notice that the tachometer dynamics complicates the matters to quite an extent. We will see that while it was relatively easy to get an acceptable bandwidth had there been no tachometer dynamics, in a real world case, the presence of tachometer dynamics severely limits the controller capability. The following block diagram presents a schematic of the overall open-loop system.

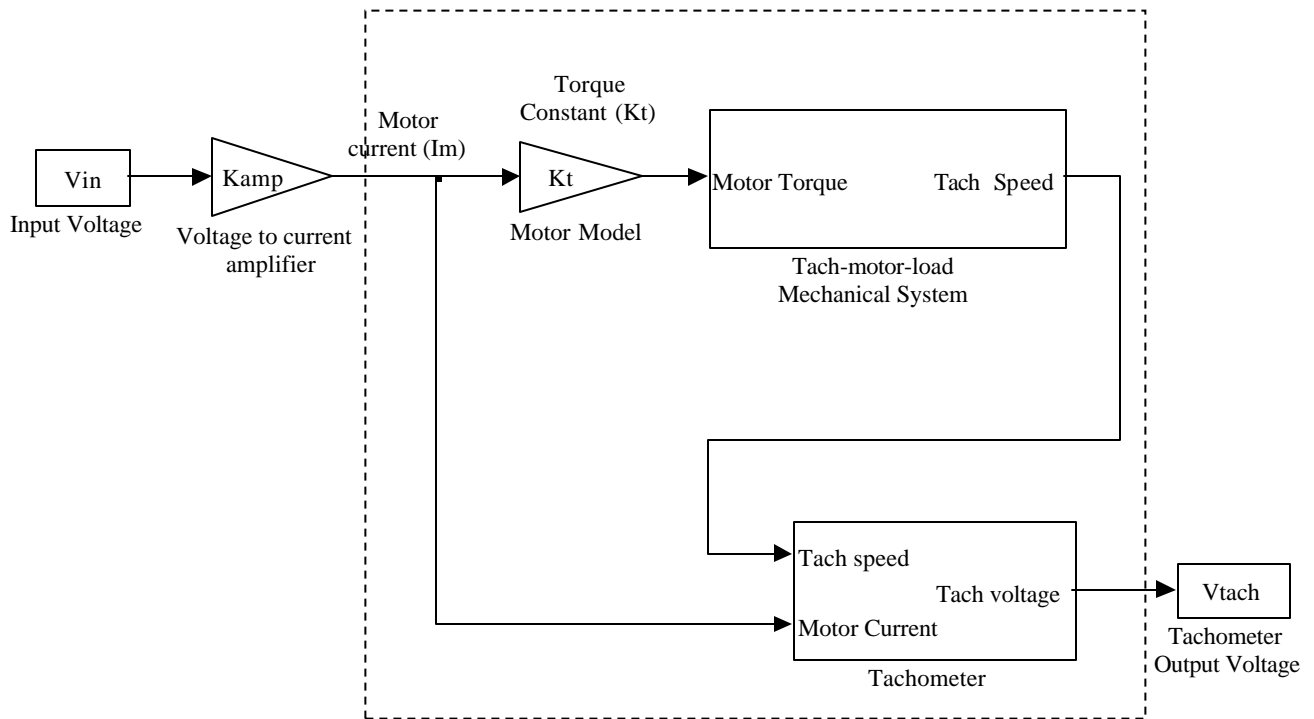


**Fig 7.20 Block-diagram based representation of the open-loop tachometer-motor-load mechanical and electrical system**

All the blocks inside the dotted square can be combined into one tachometer-motor-load system that includes both the mechanical as well as electromagnetic model of the entire system.

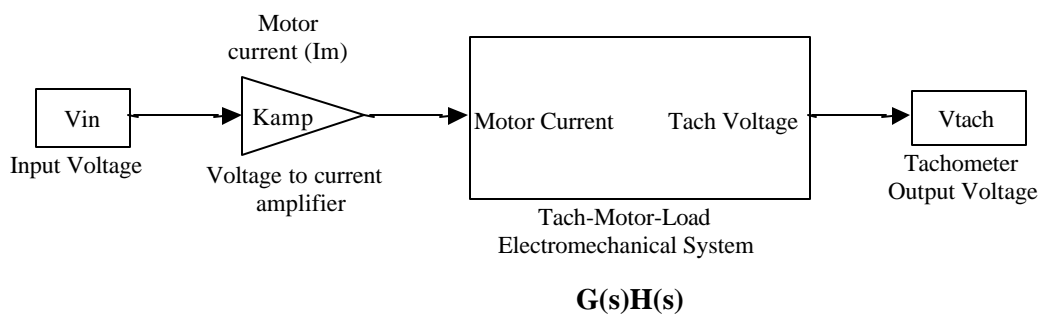


**Fig. 7.21 The tachometer-motor-load electromechanical system**

The tachometer output does not represent the actual tachometer speed since the signal has been adulterated due to tachometer dynamics. Therefore the tachometer output gives us a ‘measured’ speed, which is different from the actual speed. When the system is operated in closed loop, it can be described by the following block diagram,

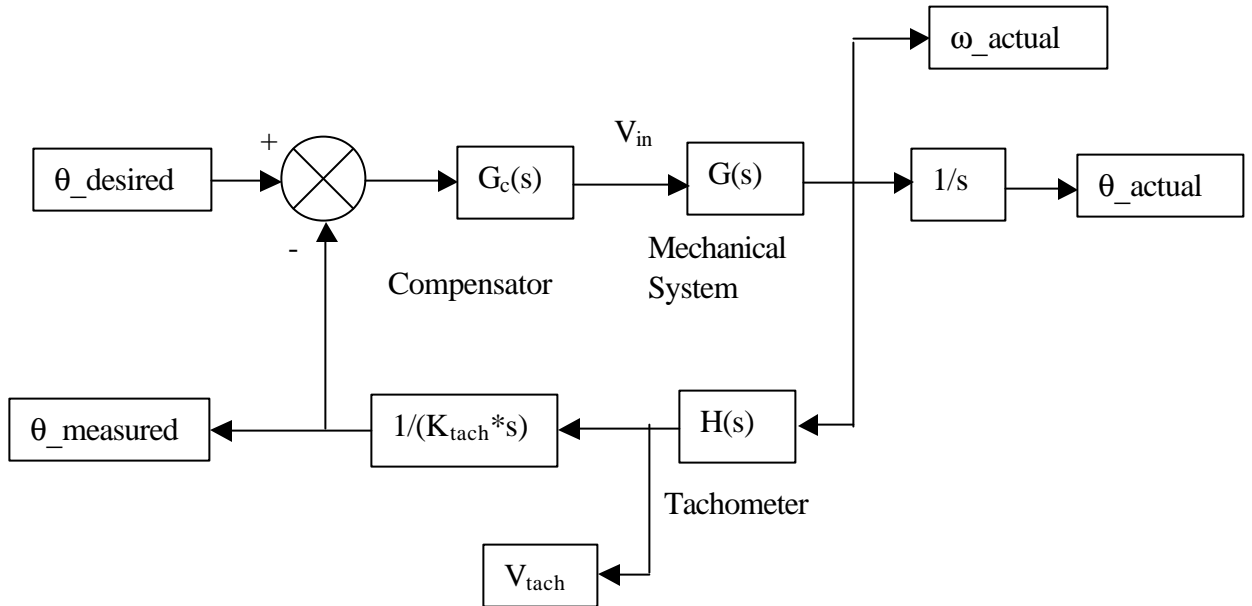


**Fig. 7.22 Close-loop block diagram of the tachometer-motor-load electromechanical system**

$G(s)H(s)$  is the overall open-loop system function, and is equal to  $V_{tach}/V_{in}$

The close-loop transfer function is then,

$$\frac{q_{actual}}{q_{desired}} = \frac{G_c(s) \left( \frac{G(s)}{s} \right)}{1 + G_c(s) \left( \frac{G(s)H(s)}{K_{tach}s} \right)}$$

where,

$$\frac{G(s)H(s)}{s} = \frac{V_{tach}}{s V_{in}} = \frac{K_{amp} [K_m s^2 (den) - K_r s (den) + K_t K_{tach} (num)]}{s^2 (den)}$$

Plugging the parameter values listed in Table 6.1, this open-loop transfer function yields the following open-loop poles and zeros. The open-loop gain is 58.

Poles	Zeros
0	118.5 + 1060i
0	118.5 - 1060i
-25 + 2615i	31.8 + 2814i
-25 - 2615i	31.8 - 2814i
-10 + 5406i	2 + 5419i
-10 - 5406i	2 - 5419i
-25 + 14019i	-2.3 + 13934i
-25 - 14019i	-2.3 - 13934i

Figures 23(a) and 23(b) provide the root-locus and Bode plots respectively for the uncompensated tachometer-motor-load electromechanical system, with the new tachometer model incorporated.

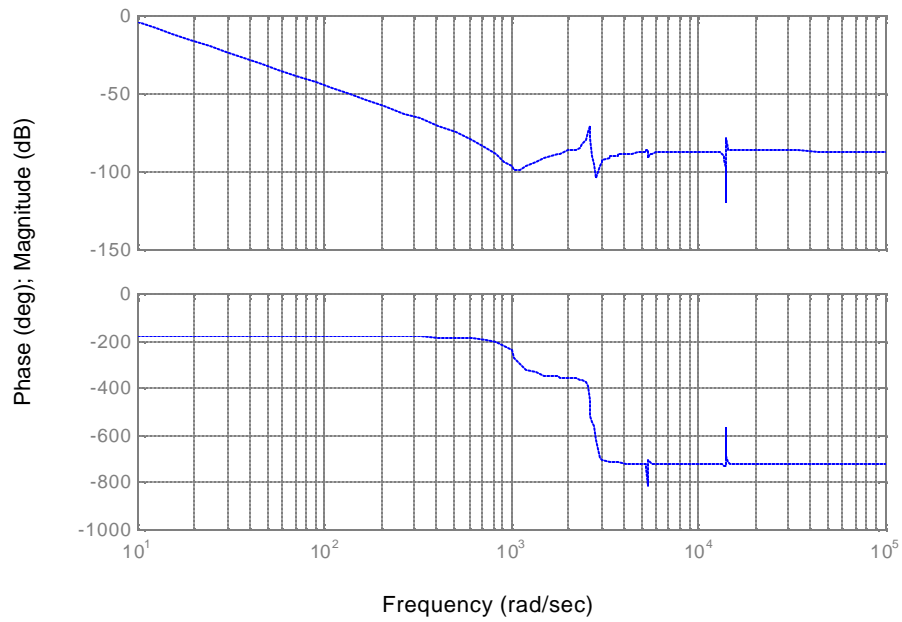
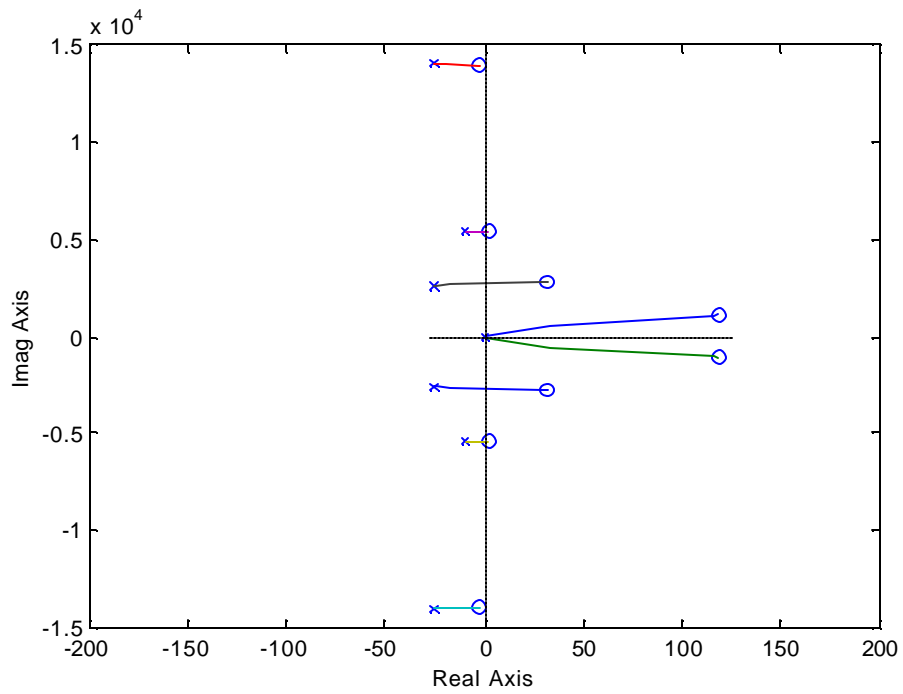


**Fig. 7.23 (a) Root-locus plot (b) Bode plots for the uncompensated system**

Because of the open-loop zeros on the right hand side of the plane the uncompensated system is always unstable in close-loop for however low gains. From the bode plots it is evident that the phase margin approaches zero for low gains but is never positive. The fact that there is pole-zero flipping doesn't have too much of an influence since the pole and zero are very closely placed.

Next we investigate the influence of a lead controller on the stability of the system.

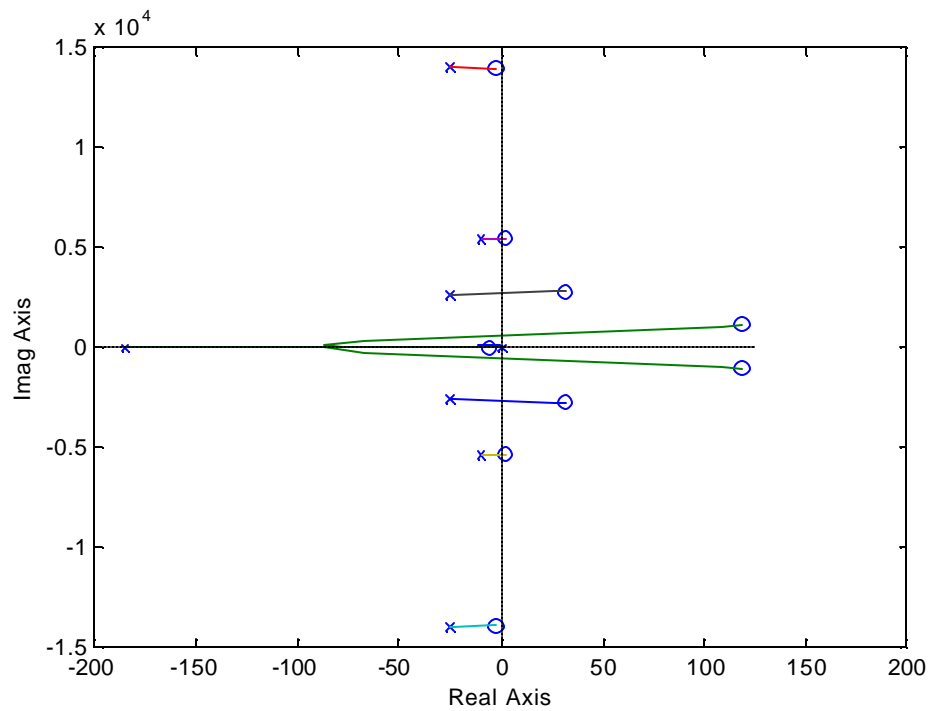


**Fig. 7.24(a) Root-locus plot for the lead compensated tachometer-motor-load electromechanical system**

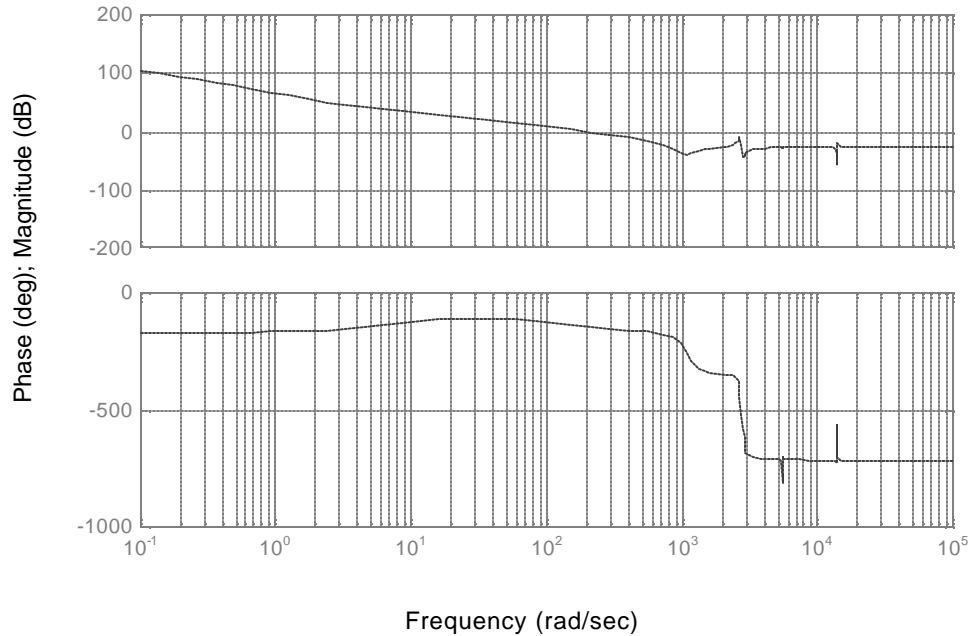


**Fig. 7.24(b) Bode plots for the lead compensated tachometer-motor-load electromechanical system**

These plots reveal some interesting information. The root-locus plots tells us that the system is close-loop stable only up till a certain value of gain, beyond which the root loci branches spill over into the right-hand side of the s-plane. This is confirmed from the Bode plots. The crossover frequency can be raised only to a certain extent, by increasing the gain, beyond which the phase margin becomes negative. Since this is a non-minimum phase system, it is phase-deficient and hence the simple lead compensator is only of limited help. Nevertheless, a bandwidth of approximately 200rad/sec is realizable as shown in the above case, using the following lead compensator,

$$20 \frac{s + 6}{s + 185}$$

Once again, the settling time is limited by the location of the closest pole-zero pair, as was explained earlier. One influence of the tachometer on the open-loop system is that it

brings the smallest zero closer to the origin. Consequently, the resulting close-loop pole is closer to the origin, thereby increasing the settling time marginally. Overall the tachometer dynamics has a deteriorating effect on the close-loop performance of the tachometer-motor-load system. To achieve better time-response characteristics, it is essential to look into other possible controller designs. Clearly a notch-filter is of no use in this case. The possibility of using a state-space controller can be explored.

## 8. CONCLUDING REMARKS AND FUTURE WORK

The conventional DC tachometer model was found to be inadequate for predicting the high-frequency responses, in cases when the tachometer is integrated with a DC motor. This led to the investigation of a more accurate tachometer model. Based on fundamental principles of electromagnetism, a new tachometer model was derived that includes the effects of mutual inductance between motor and tachometer windings, and the loading of the tachometer. In the high frequency domain, the tachometer can no longer be treated as a simple gain; it introduces some additional zeros in the feedback path. This leads to interesting consequences that are described in this thesis.

It is shown that, if high-speed servo-control is desired, the tachometer dynamics can play a significant role in the control system design. Since the tachometer-motor-load system is a multiple inertia system with multiple flexible elements, the concepts of colocated and noncolocated controls are revisited. The physical interpretation of poles and zeros in colocated and noncolocated transfer functions are sought using a simple system. These concepts are then extended to the case at hand. Once the mechanical system has been understood, the influence of tachometer dynamics on the overall system is discussed. The tachometer dynamics makes the system non-minimum phase, which makes the control-system design more complicated. It is found that the tachometer dynamics limits the performance of the close-loop system when lead controller is used. The bandwidth of the overall system cannot be increased beyond a certain limit without risking the system stability.

For future work, it is a very good exercise to design a robust state-space controller for this system that may allow for better a time-domain performance. Also it would be very instructive to build an experimental multiple-mass and multiple-spring system (preferably a four-mass three-spring system). This would be of much help in developing a physical understanding of poles and zeros of such a system. Without an actual experimental test-bed, it is difficult to visualize the various resonance modes for such a system, since a resonance mode in general involves resonance in more than one spring.

With reference to new tachometer model, some observations that are not modeled are also presented. A slight droop observed in the experimental phase plot may be due to dead time effect towards the higher frequency range. This effect is not included in the model.

Also, we have not accounted for any dynamics associated with the drive circuitry including servo amplifier. We developed the system model assuming that the drive circuitry has infinite bandwidth. A comparison of the predictions of this model with the experimental results showed little discrepancy. Based on this, we concluded that for the frequency range over which we are testing the system, the assumption regarding the driver dynamics is acceptable. The slight droop in the phase plot, mentioned earlier, may be due to a small delay time associated with the drive circuit.

During the derivation of system transfer functions, we have neglected mechanical damping. This is justified by the argument that mechanical damping does not affect the existence of system poles and zeros; it only reduces their intensity.

The purpose of this research was to point out an important electromagnetic phenomenon, which shouldn't be neglected without due consideration. It can significantly affect the system performance. The tachometer dynamics is certainly not negligible because the first tachometer-induced zero occurs much before the first system pole. But, the tachometer dynamics identified in this thesis is extremely sensitive because  $K_m$  and  $K_r$  can vary from case to case and this change can significantly alter the high-frequency system dynamics.

## REFERENCES

1. Fitzgerald, A.E. and Kingsley, C., 1961, *Electric Machinery: The Dynamics and Statics of Electromechanical Energy Conversion*, McGraw-Hill Book Company.
2. Sen, P.C., 1989, *Principles of Electric Machines and Power Electronics*, John Wiley & Sons.
3. McLean, D., 1978, "Mathematical Models of Electrical Machines," *Measurement and Control*, Vol. 11, June, pp. 231-236.
4. Welch Jr., R.H., "Mechanical Resonance in a Closed Loop Servo System", Tutorial for Motion Control Expo.
5. Ogata, K., 1998, *Modern Control Engineering*, Prentice-Hall
6. Cannon, R.H. Jr., and Rosenthal, D.E., 1984, "Experiments in Control of Flexible Structures with Noncolocated Sensors and Actuators," *Journal of Guidance*, Vol.7, No.5, Oct., pp. 546-553.
7. Miu, D.K., 1991, "Physical Interpretation of Transfer Functions Zeros for Simple Control Systems With Mechanical Flexibilities," *ASME Journal of Dynamics Systems, Measurement and Control*, Vol.113, Sept., pp. 419-424.
8. Spector, V., and Flashner, H., 1990, "Modeling and Design Implications of Noncolocated Control in Flexible Systems," *ASME Journal of Dynamics Systems, Measurement and Control*, Vol.112, June, pp. 186-163.
9. Friedland, B., 1996, *Advanced Control System Design*, Prentice-Hall
10. Franklin, G.F. and Powell, J.D., 1994, *Feedback Control of Dynamic Systems*, Addison-Wesley Publishing Company